ESAIM: M2AN 57 (2023) 467–490
https://doi.org/10.1051/m2an/2022093

**ESAIM: Mathematical Modelling and Numerical Analysis**
www.esaim-m2an.org

# AN EMA-CONSERVING, PRESSURE-ROBUST AND RE-SEMI-ROBUST METHOD WITH A ROBUST RECONSTRUCTION METHOD FOR NAVIER–STOKES ⋆

Xu Li and Hongxing Rui*

**Abstract.** Proper EMA-balance (balance of kinetic energy, linear momentum and angular momentum), pressure-robustness and Re-semi-robustness (*Re*: Reynolds number) are three important properties of Navier–Stokes simulations with exactly divergence-free elements. This EMA-balance makes a method conserve kinetic energy, linear momentum and angular momentum in an appropriate sense; pressure-robustness means that the velocity errors are independent of the pressure; Re-semi-robustness means that the constants appearing in the error bounds of kinetic and dissipation energies do not explicitly depend on inverse powers of the viscosity. In this paper, based on the pressure-robust reconstruction framework and certain suggested reconstruction operators in Linke and Merdon [*Comput. Methods Appl. Mech. Eng.* **311** (2016) 304–326], we propose a reconstruction method for a class of non-divergence-free simplicial elements which admits almost all the above properties. The only exception is the energy balance, where kinetic energy should be replaced by a suitably redefined discrete energy. The lowest order case is the Bernardi–Raugel element on general shape-regular meshes. Some numerical comparisons with exactly divergence-free methods, the original pressure-robust reconstruction methods and the EMAC method are provided to confirm our theoretical results.

**Mathematics Subject Classification.** 65M12, 65M15, 65M60, 76D05, 76D17.

Received May 11, 2022. Accepted November 14, 2022.

## 1. Introduction

In this paper, we study the finite element methods for the unsteady Navier–Stokes equations (NSEs):

$$\boldsymbol{u}_t - \nu\Delta\boldsymbol{u} + (\boldsymbol{u}\cdot\nabla)\boldsymbol{u} + \nabla p = \boldsymbol{f} \qquad \text{in } J\times\Omega, \tag{1.1a}$$

$$\nabla\cdot\boldsymbol{u} = 0 \qquad \text{in } J\times\Omega, \tag{1.1b}$$

$$\boldsymbol{u}(0) = \boldsymbol{u}^0 \qquad \text{in } \Omega, \tag{1.1c}$$

$$\boldsymbol{u} = \boldsymbol{0} \qquad \text{on } J\times\Gamma, \tag{1.1d}$$

*Keywords and phrases.* Finite element methods, unsteady Navier–Stokes equations, pressure-robustness, EMAC formulation, Re-semi-robustness.

⋆ *Partial work was completed during the first author's visit at Weierstrass Institute, 10117 Berlin, Germany.*

School of Mathematics, Shandong University, Jinan 250100, P.R. China.
*Corresponding author: hxrui@sdu.edu.cn

where $J = (0, T]$ is a bounded time interval, $\Omega \subset \mathbb{R}^d$ $(d = 2, 3)$ is a bounded domain with Lipschitz-continuous polyhedral boundary $\Gamma$, $\boldsymbol{u}$ and $p$ represent the velocity and pressure unknowns, $\nu > 0$ is the constant kinematic viscosity, $\boldsymbol{f}$ represents the external force, and $\boldsymbol{u}^0$ is the initial velocity. We assume $\boldsymbol{f}(t) \in \boldsymbol{L}^2(\Omega)$ for all $t \in J$.

For designing accurate numerical schemes, it is widely believed that preserving the fundamental (physical or mathematical) properties of the continuous problem is of great importance. For NSEs, these fundamental properties include the divergence constraint (1.1b), the balance laws for some physical quantities (*e.g.*, kinetic energy, linear momentum, angular momentum, vorticity, helicity, and enstrophy) [12, 19], and an invariance property for the velocity with respect to the gradient field in $\boldsymbol{f}$ [34, 41]. Among these properties, the divergence constraint is of central importance. The papers [19, 34] showed that exactly divergence-free mixed methods preserve the balance laws and the invariance property mentioned above. The latter means that these methods are pressure-robust; namely the velocity errors are independent of the pressure. Moreover, it was demonstrated in [55] that the constants in error estimates, including the Gronwall constant, did not depend on $\nu^{-1}$ explicitly for divergence-free finite element methods. This property was called (Re-)semi-robustness, uniform, or quasi-uniform estimates [35] sometimes.

Due to these fascinating properties, constructing exactly divergence-free elements has been an increasingly hot topic in recent years [14, 28–30, 46, 47, 58]. However, compared to classical non-divergence-free elements, the construction of these elements is not trivial in most cases. For example, the well-known $d$-th order Scott–Vogelius elements usually require a barycentric-refined mesh.

Another popular idea is relaxing the continuity condition but enforcing the divergence constraint strongly, which results in the so-called nonconforming $H(\mathrm{div})$-conforming methods [15, 27, 36, 53, 56, 57]. In this paper, we focus on the conforming mixed methods for the Navier–Stokes equations.

Modifying the formulation to preserve some fundamental properties of the continuous problem (or divergence-free mixed methods) for non-divergence-free elements is another popular research topic. With an observation that most classical elements are non-divergence-free, this topic includes, but is not limited to, pressure-robust reconstructions [37, 38, 40, 41, 43, 45], the EMAC (EMA-conserving) formulation [12, 13, 49], and some Re-semi-robust methods [3, 10, 16, 17, 23].

The method introduced in this paper is also included in this topic. Pressure-robustness plays an important role on the accuracy of a method when *"gradient forces dominate the momentum balance"* [44]; the velocity errors of the methods which are not Re-semi-robust might grow quickly with respect to time for higher Reynolds number flows [55]; the EMAC scheme is one of the "enhanced-physics" based schemes which have a long history such as [1, 4, 20, 51, 52], and the paper [49] showed that an improper treatment of energy, linear momentum and angular momentum produced lower bounds for $L^2$ velocity error. It is worth mentioning that, the properties mentioned above are usually not mutually independent. For example, in the paper [49], Olshanskii and Rebholz proved that the Gronwall constants in EMAC estimates did not depend on the viscosity explicitly, which was exactly Re-semi-robustness except that the constant related to a pressure-induced error term polynomially depended on the inverse of viscosity. Another example is the popular grad-div stabilization [11, 48, 50]. It can not only weaken the impact of the pressure on velocity errors [34, 48] but also make the usual skew-symmetric scheme Re-semi-robust [16]. Finally, we also refer the readers to the review articles [22, 34, 35] for more details.

In this paper, we propose a reconstruction formulation which is EMA-conserving for the reconstructed discrete velocity (here the energy should be redefined as (2.15) below), pressure-robust, and Re-semi-robust. For simplicity, we shall refer to this reconstruction method as the "EMAPR" method throughout this paper. Our method is based on the pressure-robust reconstruction formulation in [43]. The main difference lies on the discretization of the convective term. For the convective term, two pressure-robust discrete forms were proposed in [43]: the convective form and the rotational form. Following a similar strategy as in [12], one can check that these two forms do not conserve linear momentum and angular momentum (the latter conserves kinetic energy). Here we propose an EMA-conserving form, *i.e.*, it does not produce any extra energy, momentum and angular momentum in an appropriate sense. Then we give a pressure-robust and Re-semi-robust error estimate for the continuous-in-time case, provided that the continuous solution $\boldsymbol{u}$ is in $L^2\big(J; \boldsymbol{W}^{1,\infty}(\Omega)\big)$. To obtain such an estimate, we also need to slightly modify the discretization of the evolutionary term by introducing a stabilization.

Finally, we shall prove that our formulation can be easily applied to a class of simplicial locally mass-conserving elements whose pressures are discontinuous. Moreover, the reconstruction also lowers the requirement of the quadrature rules. Note that in a practical view a drawback of this class of elements is that it uses bubble functions to enrich velocity spaces which require higher order quadrature rules. To the best of our knowledge, the EMAPR method is the first method on conforming non-divergence-free elements which is EMA-conserving, pressure-robust, and Re-semi-robust simultaneously. For nonconforming and non-divergence-free methods, a reconstructed hybrid discontinuous Galerkin method in [39] (see formulas "(6.3d)" and "(6.5)" therein) probably admits most of these properties also. The lowest number of DoFs (degrees of freedom) of our method is the same as of the lowest order divergence-free methods proposed in [14,30], while our method uses simpler bubble functions which do not require any special split of meshes.

We also conjecture that the EMAC formulation with grad-div stabilization is a simple and efficient strategy in practice, as the grad-div stabilization can dramatically lower the effect of the pressure and also make a method Re-semi-robust. Moreover, in the original paper [48], it was shown that the grad-div stabilization could also improve the performance of linear algebraic solvers. However, for a much more complicated or very large pressure (which can happen in practice; *cf.* [21,42]), the grad-div stabilization might not be enough since it can not remove the the effect of the pressure totally. Some numerical comparisons on this aspect are also done in this paper.

The remainder of this paper is organized as follows. In Section 2 we discuss the EMAPR methods and some balance laws. Section 3 is devoted to a pressure-robust and Re-semi-robust error estimate for the EMAPR method. We show that a class of non-divergence-free elements can be easily incorporated into our framework in Section 4. Finally we carry out some numerical experiments in Section 5 and do some conclusions in Section 6.

In what follows we will use $C$, with or without a subscript, to denote a generic positive constant. The standard inner product for $\left[L^2(D)\right]^n$ or $\left[L^2(D)\right]^{n\times n}$ $(n \in \mathbb{Z})$ will be denoted by $(\cdot,\cdot)_D$ uniformly. The notation $\|\cdot\|_{m,p,D}$ ($|\cdot|_{m,p,D}$) will be used to denote the Sobolev norm (seminorm, respectively) of $[W^{m,p}(D)]^n$ or $[W^{m,p}(D)]^{n\times n}$. With the convention the subscripts $m, p$ and $D$ will be omitted for $m = 0$, $p = 2$ and $D = \Omega$, respectively. $H^m(D)$ coincides with $W^{m,2}(D)$ and $\boldsymbol{W}^{m,p}(D)$ coincides with $[W^{m,p}(D)]^d$.

## 2. The EMAPR reconstruction method

### 2.1. The divergence-free reconstruction operator

Let $\mathcal{T}_h$ denote a partition of $\Omega$. We define the mesh size $h := \max_{K\in\mathcal{T}_h} h_K$ with $h_K$ the diameter of elements $K$. Denote by $\varrho_K$ the diameter of the biggest ball inscribed in $K$. Here we assume that $\mathcal{T}_h$ is shape-regular, *i.e.*, there exists a positive constant $\xi$ such that

$$\frac{h_K}{\varrho_K} \le \xi \quad \forall K \in \mathcal{T}_h. \tag{2.1}$$

We define

$$\begin{aligned} \boldsymbol{V} &:= \boldsymbol{H}_0^1(\Omega) = \left\{\boldsymbol{v} \in \boldsymbol{H}^1(\Omega) : \boldsymbol{v}|_\Gamma = \boldsymbol{0}\right\}, \\ \boldsymbol{X} &:= \boldsymbol{H}_0(\mathrm{div};\Omega) = \{\boldsymbol{v} \in \boldsymbol{H}(\mathrm{div};\Omega) : \boldsymbol{v}\cdot\boldsymbol{n}|_\Gamma = 0\}, \\ \boldsymbol{H}^2(\mathcal{T}_h) &:= \left\{\boldsymbol{v} \in \boldsymbol{L}^2(\Omega) : \boldsymbol{v}|_K \in \boldsymbol{H}^2(K) \quad \forall K \in \mathcal{T}_h\right\}, \end{aligned}$$

and

$$W = L_0^2(\Omega) := \left\{q \in L^2(\Omega) : \int_\Omega q \,\mathrm{d}\boldsymbol{x} = 0\right\},$$

where $\boldsymbol{n}$ is the unit external normal vector on $\Gamma$. Furthermore we define the bilinear form $b : \boldsymbol{X} \times W \to \mathbb{R}$ by

$$b(\boldsymbol{v}, q) := (\nabla\cdot\boldsymbol{v}, q) \quad \text{for any} \quad (\boldsymbol{v}, q) \in \boldsymbol{X} \times W.$$

Let $(\boldsymbol{V}_h, \boldsymbol{X}_h, W_h) \subset (\boldsymbol{V}, \boldsymbol{X}, W)$ denote a triple of finite element spaces satisfying

$$\inf_{q_h \in W_h} \sup_{\boldsymbol{v}_h \in \boldsymbol{V}_h \setminus \{\boldsymbol{0}\}} \frac{b(\boldsymbol{v}_h, q_h)}{\|\nabla \boldsymbol{v}_h\|} \geq \beta_h \text{ for some } \beta_h > 0 \tag{2.2}$$

and

$$\nabla \cdot \boldsymbol{X}_h \subseteq W_h. \tag{2.3}$$

Denote by

$$\boldsymbol{V}^0 := \{\boldsymbol{v} \in \boldsymbol{V} : b(\boldsymbol{v}, q) = 0 \quad \forall q \in W\} = \{\boldsymbol{v} \in \boldsymbol{V} : \nabla \cdot \boldsymbol{v} = 0\}$$

and

$$\boldsymbol{V}_h^0 := \{\boldsymbol{v}_h \in \boldsymbol{V}_h : b(\boldsymbol{v}_h, q_h) = 0 \quad \forall q_h \in W_h\}$$

the spaces of divergence-free velocity functions and discretely divergence-free velocity functions, respectively. Note that if $\nabla \cdot \boldsymbol{V}_h \subseteq W_h$, we have $\boldsymbol{V}_h^0 \subset \boldsymbol{V}^0$, which means that the functions in $\boldsymbol{V}_h^0$ are exactly divergence-free. For most classical elements, this relationship does not hold.

Let $P_k(K)$ denote the space of polynomials on $K$ of degree no more than $k$. We also define

$$\boldsymbol{P}_k := \left\{\boldsymbol{v}_h \in \boldsymbol{V} : \boldsymbol{v}_h|_K \in [P_k(K)]^d \text{ for all } K \in \mathcal{T}_h\right\}.$$

We suppose that the velocity space $\boldsymbol{V}_h$ is of order $k$ ($k \geq 1$), *i.e.*, there exists a non-negative integer $k$ such that $\boldsymbol{P}_k \subset \boldsymbol{V}_h$ and $\boldsymbol{P}_{k+1} \not\subset \boldsymbol{V}_h$.

We assume the existence of a divergence-free reconstruction operator $\Pi_h : \boldsymbol{V}_h \to \boldsymbol{X}_h$ (we do not give the detailed definition here) which satisfies that

$$\nabla \cdot \Pi_h \boldsymbol{v}_h \equiv 0 \qquad \text{for all } \boldsymbol{v}_h \in \boldsymbol{V}_h^0, \tag{2.4}$$

$$b(\boldsymbol{v}_h, q_h) = b(\Pi_h \boldsymbol{v}_h, q_h) \qquad \text{for all } (\boldsymbol{v}_h, q_h) \in \boldsymbol{V}_h \times W_h, \tag{2.5}$$

and

$$(\boldsymbol{g}, \boldsymbol{v}_h - \Pi_h \boldsymbol{v}_h) \leq C h^k |\boldsymbol{g}|_{k-1} \|\nabla \boldsymbol{v}_h\| \text{ for all } \boldsymbol{g} \in \boldsymbol{H}^{k-1}(\Omega), \boldsymbol{v}_h \in \boldsymbol{V}_h^0. \tag{2.6}$$

Note that (2.4) can be derived from (2.3) and (2.5).

We also assume that $\Pi_h$ satisfies the following properties.

**Assumption 1.** *There exist two operators $\Pi_h^1 : \boldsymbol{V}_h \to \boldsymbol{V}_h$ and $\Pi_h^{\mathrm{R}} : \boldsymbol{V}_h \to \boldsymbol{X}_h$ and two positive constants $C_{1,\infty}$ and $C_{\mathrm{R},\infty}$ such that $\Pi_h \boldsymbol{v}_h = \Pi_h^1 \boldsymbol{v}_h + \Pi_h^{\mathrm{R}} \boldsymbol{v}_h$ for all $\boldsymbol{v}_h \in \boldsymbol{V}_h$ and*

$$|\Pi_h^1 \boldsymbol{v}_h|_{1,\infty,K} \leq C_{1,\infty} |\boldsymbol{v}_h|_{1,\infty,K} \qquad \forall K \in \mathcal{T}_h, \boldsymbol{v}_h \in \boldsymbol{V}_h^0, \tag{2.7}$$

$$\|\Pi_h^{\mathrm{R}} \boldsymbol{v}_h\|_{\infty,K} \leq C_{\mathrm{R},\infty} h_K |\boldsymbol{v}_h|_{1,\infty,K} \qquad \forall K \in \mathcal{T}_h, \boldsymbol{v}_h \in \boldsymbol{V}_h^0. \tag{2.8}$$

**Remark 1.** The fundamental requirement of the projection $\Pi_h$ is: For any $\boldsymbol{v}_h \in \boldsymbol{V}_h$, $\Pi_h \boldsymbol{v}_h$ can be decomposed into a sufficiently approximate $H^1$-conforming component and a "small" $H(\mathrm{div})$-conforming component (consider $\Pi_h^1 \boldsymbol{v}_h$ and $\Pi_h^{\mathrm{R}} \boldsymbol{v}_h$). This is the prerequisite to constructing our methods. Regarding the discretization of the convection term (see (2.14) below), a rough description of our basic idea is: Apply the $H^1$-conforming part to guarantee the accuracy and "abuse" the $H(\mathrm{div})$-conforming part to guarantee the conservation of energy, momentum and angular momentum. In Section 4, we shall show that the reconstruction operators in Remark 4.2 of [43] and their higher order versions on a class of non-divergence-free simplicial elements satisfy all the above properties.

### 2.2. The EMAPR method for classical elements

Define

$$a(\boldsymbol{u},\boldsymbol{v}) := (\nabla\boldsymbol{u},\nabla\boldsymbol{v}) \text{ for all } \boldsymbol{u},\boldsymbol{v}\in\boldsymbol{V}$$

and the convective trilinear form (CONV)

$$c(\boldsymbol{u},\boldsymbol{v},\boldsymbol{w}) := ((\boldsymbol{u}\cdot\nabla)\boldsymbol{v},\boldsymbol{w}) \text{ for all } (\boldsymbol{u},\boldsymbol{v},\boldsymbol{w})\in\boldsymbol{L}^2(\Omega)\times\boldsymbol{V}\times\boldsymbol{L}^2(\Omega).$$

The weak formulation for (1.1) characterizes $(\boldsymbol{u},p): J\to\boldsymbol{V}\times W$ by

$$(\partial_t\boldsymbol{u},\boldsymbol{v})+\nu a(\boldsymbol{u},\boldsymbol{v})+c(\boldsymbol{u},\boldsymbol{u},\boldsymbol{v})-b(\boldsymbol{v},p)=(\boldsymbol{f},\boldsymbol{v}) \qquad \forall\boldsymbol{v}\in\boldsymbol{V}, \tag{2.9a}$$

$$b(\boldsymbol{u},q)=0 \qquad \forall q\in W, \tag{2.9b}$$

and $\boldsymbol{u}(0)=\boldsymbol{u}^0$. A straightforward semi-discrete analog of (2.9) is to find $(\boldsymbol{u}_h,p_h): J\to\boldsymbol{V}_h\times W_h$ satisfying $\boldsymbol{u}_h(0)=\boldsymbol{u}_h^0\in\boldsymbol{V}_h$ with $\boldsymbol{u}_h^0$ being some approximation of $\boldsymbol{u}^0$ and

$$(\partial_t\boldsymbol{u}_h,\boldsymbol{v}_h)+\nu a(\boldsymbol{u}_h,\boldsymbol{v}_h)+c(\boldsymbol{u}_h,\boldsymbol{u}_h,\boldsymbol{v}_h)-b(\boldsymbol{v}_h,p_h)=(\boldsymbol{f},\boldsymbol{v}_h), \tag{2.10a}$$

$$b(\boldsymbol{u}_h,q_h)=0, \tag{2.10b}$$

for all $(\boldsymbol{v}_h,q_h)\in\boldsymbol{V}_h\times W_h$. However, it is well-known that the above scheme is not energy-stable and pressure-robust unless $\boldsymbol{u}_h$ is exactly divergence-free (or equivalently, $\nabla\cdot\boldsymbol{V}_h\subseteq W_h$). To obtain a pressure-robust velocity for classical elements, in [43] Linke and Merdon proposed a novel finite element formulation which reads

$$\begin{aligned}(\Pi_h\partial_t\boldsymbol{u}_h,\Pi_h\boldsymbol{v}_h)+\nu a(\boldsymbol{u}_h,\boldsymbol{v}_h)+c(\boldsymbol{u}_h,\boldsymbol{u}_h,\Pi_h\boldsymbol{v}_h)-b(\boldsymbol{v}_h,p_h)&=(\boldsymbol{f},\Pi_h\boldsymbol{v}_h),\\ b(\boldsymbol{u}_h,q_h)&=0.\end{aligned}$$

Here $b(\boldsymbol{v}_h,p_h)$ should be interpreted as $b(\Pi_h\boldsymbol{v}_h,p_h)$ *via* property (2.5). By using divergence-free reconstructions, the above formulation restores the $L^2$-orthogonality between discretely divergence-free test functions and gradient fields, and thus remove the effect of the continuous pressure in velocity errors. There is some consistency error arising from the diffusion term.

To make the method energy-stable, a pressure-robust and energy-conserving rotational form (ROT) of the nonlinear term was also proposed in [43]:

$$c_{\mathrm{rot}}(\boldsymbol{u}_h,\boldsymbol{v}_h,\boldsymbol{w}_h) := (\nabla\times\boldsymbol{u}_h\times\Pi_h\boldsymbol{v}_h,\Pi_h\boldsymbol{w}_h), \tag{2.11}$$

where $\nabla\times$ is the curl operator [25]. However, following the strategy in [12] or Section 2.3 below, one can prove that the rotational form does not preserve momentum and angular momentum (see Rem. 3 below). To resolve this issue, we propose an EMA-conserving form, which results in the EMAPR reconstruction:

Find $(\boldsymbol{u}_h,p_h): J\to\boldsymbol{V}_h\times W_h$ such that

$$d_h(\partial_t\boldsymbol{u}_h,\boldsymbol{v}_h)+\nu a(\boldsymbol{u}_h,\boldsymbol{v}_h)+c_h(\boldsymbol{u}_h,\boldsymbol{u}_h,\boldsymbol{v}_h)-b(\boldsymbol{v}_h,p_h)=(\boldsymbol{f},\Pi_h\boldsymbol{v}_h), \tag{2.12a}$$

$$b(\boldsymbol{u}_h,q_h)=0, \tag{2.12b}$$

for all $\boldsymbol{v}_h\in\boldsymbol{V}_h, q_h\in W_h$ and $\boldsymbol{u}_h(0)=\boldsymbol{u}_h^0$. Here $d_h$ is given by

$$d_h(\boldsymbol{u}_h,\boldsymbol{v}_h) := (\Pi_h\boldsymbol{u}_h,\Pi_h\boldsymbol{v}_h)+\alpha\big(\Pi_h^{\mathrm{R}}\boldsymbol{u}_h,\Pi_h^{\mathrm{R}}\boldsymbol{v}_h\big), \tag{2.13}$$

where $\alpha$ is a positive parameter. The trilinear form $c_h$ is defined by

$$\begin{aligned}c_h(\boldsymbol{u}_h,\boldsymbol{v}_h,\boldsymbol{w}_h) &:= c\big(\Pi_h\boldsymbol{u}_h,\Pi_h^1\boldsymbol{v}_h,\Pi_h^1\boldsymbol{w}_h\big)+c\big(\Pi_h\boldsymbol{u}_h,\Pi_h^1\boldsymbol{v}_h,\Pi_h^{\mathrm{R}}\boldsymbol{w}_h\big)-c\big(\Pi_h\boldsymbol{u}_h,\Pi_h^1\boldsymbol{w}_h,\Pi_h^{\mathrm{R}}\boldsymbol{v}_h\big)\\ &= c\big(\Pi_h\boldsymbol{u}_h,\Pi_h^1\boldsymbol{v}_h,\Pi_h\boldsymbol{w}_h\big)-c\big(\Pi_h\boldsymbol{u}_h,\Pi_h^1\boldsymbol{w}_h,\Pi_h^{\mathrm{R}}\boldsymbol{v}_h\big).\end{aligned} \tag{2.14}$$

**Remark 2.** The bilinear form $d_h$ with $\alpha = 0$ is commonly used in pressure-robust reconstructions for the $(\boldsymbol{u}, \boldsymbol{v})$-like term [2, 43]. However, for the case $\alpha = 0$ we can not obtain a Re-semi-robust estimate theoretically. In practice, we find that the stabilization term $\left(\Pi_h^{\mathrm{R}}\boldsymbol{u}_h, \Pi_h^{\mathrm{R}}\boldsymbol{v}_h\right)$ is of importance for high order elements ($k \geq 2$) in the case that $\nu$ is very small or equal to zero (the Euler equation). In this case, without this term, the $\boldsymbol{H}^1$ error of the discrete velocity might be large.

### 2.3. EMA-balance in semi-discrete schemes

Now we are in the position to analyze the balance laws with the EMAPR reconstruction. We define kinetic energy $E : \boldsymbol{X} \to \mathbb{R}$, linear momentum $M : \boldsymbol{X} \to \mathbb{R}^d$, and angular momentum $M_{\boldsymbol{x}} : \boldsymbol{X} \to \mathbb{R}^3$ by

$$E(\boldsymbol{u}^*) := \frac{1}{2}\int_\Omega |\boldsymbol{u}^*|^2 \,\mathrm{d}\boldsymbol{x}, \quad M(\boldsymbol{u}^*) := \int_\Omega \boldsymbol{u}^* \,\mathrm{d}\boldsymbol{x}, \quad M_{\boldsymbol{x}}(\boldsymbol{u}^*) := \int_\Omega \boldsymbol{u}^* \times \boldsymbol{x} \,\mathrm{d}\boldsymbol{x},$$

for any $\boldsymbol{u}^* \in \boldsymbol{X}$. For any two-dimensional vector $\boldsymbol{u}^* = (u_1^*, u_2^*)$, to compute angular momentum or cross product, one can always embed it into three dimensions by setting $\boldsymbol{u}^* = (u_1^*, u_2^*, 0)$. Let $\boldsymbol{u}$ be the solution of (2.9) which satisfies the following balance laws [12, 49]:

$$\frac{\mathrm{d}}{\mathrm{d}t}E(\boldsymbol{u}) + \nu\|\nabla\boldsymbol{u}\|^2 = (\boldsymbol{f}, \boldsymbol{u}), \quad \frac{\mathrm{d}}{\mathrm{d}t}M(\boldsymbol{u}) = \int_\Omega \boldsymbol{f} \,\mathrm{d}\boldsymbol{x}, \quad \frac{\mathrm{d}}{\mathrm{d}t}M_{\boldsymbol{x}}(\boldsymbol{u}) = \int_\Omega \boldsymbol{f} \times \boldsymbol{x} \,\mathrm{d}\boldsymbol{x},$$

where the balance laws of momentum and angular momentum are based on some appropriate assumptions. Similarly to the assumptions in [12, 13, 49], here (only for the analysis of momentum and angular momentum) we assume that $(\boldsymbol{u}, p)$ is compactly supported in $\Omega$ (*e.g.*, consider an isolated vortex). We also define a discrete energy $E_d : \boldsymbol{V}_h^0 \to \mathbb{R}$ by

$$E_d(\boldsymbol{u}^*) := \frac{1}{2}d_h(\boldsymbol{u}^*, \boldsymbol{u}^*), \tag{2.15}$$

for any $\boldsymbol{u}^* \in \boldsymbol{V}_h^0$, which is asymptotically convergent to the real energy. Note that we have $E(\Pi_h\boldsymbol{u}^*) \leq E_d(\boldsymbol{u}^*)$.

The following lemma is essential for EMA analysis.

**Lemma 1.** *For any finite element triple* $(\boldsymbol{u}_h, \boldsymbol{v}_h, \boldsymbol{w}_h) \in \boldsymbol{H}(\mathrm{div}; \Omega) \times \boldsymbol{H}^1(\Omega) \times \boldsymbol{H}^1(\Omega)$, *we have*

$$c(\boldsymbol{u}_h, \boldsymbol{v}_h, \boldsymbol{w}_h) = -c(\boldsymbol{u}_h, \boldsymbol{w}_h, \boldsymbol{v}_h) \tag{2.16}$$

*if*

(1) $\boldsymbol{u}_h$ *is exactly divergence-free, i.e.,* $\nabla \cdot \boldsymbol{u}_h \equiv 0$;
(2) $\boldsymbol{u}_h|_\Gamma \cdot \boldsymbol{n} = 0$ *or* $\boldsymbol{v}_h|_\Gamma = \boldsymbol{0}$ *or* $\boldsymbol{w}_h|_\Gamma = \boldsymbol{0}$.

*Proof.* Integration by parts over an element $K \in \mathcal{T}_h$ yields

$$\int_K (\boldsymbol{u}_h \cdot \nabla)\boldsymbol{v}_h \cdot \boldsymbol{w}_h \,\mathrm{d}\boldsymbol{x} = -\int_K (\boldsymbol{u}_h \cdot \nabla)\boldsymbol{w}_h \cdot \boldsymbol{v}_h \,\mathrm{d}\boldsymbol{x} - \int_K \nabla \cdot \boldsymbol{u}_h(\boldsymbol{v}_h \cdot \boldsymbol{w}_h) \,\mathrm{d}\boldsymbol{x} + \int_{\partial K} \boldsymbol{u}_h \cdot \boldsymbol{n}(\boldsymbol{v}_h \cdot \boldsymbol{w}_h) \,\mathrm{d}s.$$

Note that $\boldsymbol{u}_h$ is normally continuous and $\boldsymbol{v}_h$ and $\boldsymbol{w}_h$ are totally continuous, which, together with a combination of conditions (1) and (2), implies

$$c(\boldsymbol{u}_h, \boldsymbol{v}_h, \boldsymbol{w}_h) = \sum_{K\in\mathcal{T}_h} \int_K (\boldsymbol{u}_h \cdot \nabla)\boldsymbol{v}_h \cdot \boldsymbol{w}_h \,\mathrm{d}\boldsymbol{x} = -\sum_{K\in\mathcal{T}_h} \int_K (\boldsymbol{u}_h \cdot \nabla)\boldsymbol{w}_h \cdot \boldsymbol{v}_h \,\mathrm{d}\boldsymbol{x} = -c(\boldsymbol{u}_h, \boldsymbol{w}_h, \boldsymbol{v}_h).$$

This completes the proof. □

Lemma 1 and (2.14) imply the following lemma.

**Lemma 2.** *For any* $(\boldsymbol{u}_h, \boldsymbol{v}_h, \boldsymbol{w}_h) \in \boldsymbol{V}_h^0 \times \boldsymbol{V}_h \times \boldsymbol{V}_h$ *we have*

$$c_h(\boldsymbol{u}_h, \boldsymbol{v}_h, \boldsymbol{w}_h) = -c_h(\boldsymbol{u}_h, \boldsymbol{w}_h, \boldsymbol{v}_h).$$

Using a chain rule like $\partial_t(\boldsymbol{q}^2) = 2\boldsymbol{q} \cdot \partial_t \boldsymbol{q}$, we have $d_h(\partial_t \boldsymbol{u}_h, \boldsymbol{u}_h) = \frac{\mathrm{d}}{\mathrm{d}t} E_d(\boldsymbol{u}_h)$. Setting $\boldsymbol{v}_h = \boldsymbol{u}_h$ in (2.12) and applying (2.12b) and Lemma 2, one immediately obtains the following theorem.

**Theorem 1.** *Let* $\boldsymbol{u}_h$ *be the solution of* (2.12). *Then it satisfies the following balance of energy:*

$$\frac{\mathrm{d}}{\mathrm{d}t} E_d(\boldsymbol{u}_h) + \nu \|\nabla \boldsymbol{u}_h\|^2 = (\boldsymbol{f}, \Pi_h \boldsymbol{u}_h).$$

Boundary conditions may influence the balance of momentum and angular momentum. For simplicity, we ignore the effect of boundary here by doing some extra assumptions which are similar to those of the continuous case. Similar assumptions were also used for the analysis of the EMAC formulation in [12].

**Assumption 2.** *The finite element solution* $(\boldsymbol{u}_h, p_h)$, $\Pi_h \boldsymbol{u}_h$ *and the external force* $\boldsymbol{f}$ *are only supported on a sub-mesh* $\hat{\mathcal{T}}_h \subset \mathcal{T}_h$ *such that there exists an operator* $\chi : \boldsymbol{H}^1(\Omega) \to \boldsymbol{P}_k \subseteq \boldsymbol{V}_h$ *satisfying*

$$\chi(\boldsymbol{g})|_{\hat{\mathcal{T}}_h} = \boldsymbol{g}, \quad \Pi_h \chi(\boldsymbol{g})|_{\hat{\mathcal{T}}_h} = \Pi_h^1 \chi(\boldsymbol{g})|_{\hat{\mathcal{T}}_h} = \boldsymbol{g}, \tag{2.17}$$

*for* $\boldsymbol{g} = \boldsymbol{e}_i, \boldsymbol{x} \times \boldsymbol{e}_i$ $(1 \le i \le d)$. *Here* $\boldsymbol{e}_i \in \mathbb{R}^d$ *is the unit vector whose* $i$*-th component equals 1.*

In fact, for discontinuous pressure elements (like the elements we used herein), the support of $\Pi_h \boldsymbol{u}_h$ is the same as that of $\boldsymbol{u}_h$, since the reconstruction can be locally performed on each element. Furthermore, note that $\nabla \cdot \boldsymbol{e}_i = \nabla \cdot (\boldsymbol{x} \times \boldsymbol{e}_i) = 0$ and $\boldsymbol{e}_i$ and $\boldsymbol{x} \times \boldsymbol{e}_i$ are linear polynomials. So the equalities for $\Pi_h$ and $\Pi_h^1$ in (2.17) are not hard to satisfy. The reconstruction operators in Section 4 fulfill these equalities.

For any $\boldsymbol{a}, \boldsymbol{b}, \boldsymbol{c} \in \mathbb{R}^3$, the following identities will be used to analyze angular momentum:

$$\boldsymbol{a} \cdot (\boldsymbol{b} \times \boldsymbol{c}) = (\boldsymbol{a} \times \boldsymbol{b}) \cdot \boldsymbol{c}, \tag{2.18}$$

$$(\boldsymbol{a} \cdot \nabla)(\boldsymbol{x} \times \boldsymbol{e}_i) \cdot \boldsymbol{b} = -(\boldsymbol{a} \times \boldsymbol{b}) \cdot \boldsymbol{e}_i. \tag{2.19}$$

**Theorem 2.** *Let* $\boldsymbol{u}_h$ *be the solution of* (2.12). *Under Assumption 2* $\Pi_h u_h$ *satisfies*

$$\frac{\mathrm{d}}{\mathrm{d}t} M(\Pi_h \boldsymbol{u}_h) = \int_\Omega \boldsymbol{f} \, \mathrm{d}\boldsymbol{x} \quad \text{and} \quad \frac{\mathrm{d}}{\mathrm{d}t} M_{\boldsymbol{x}}(\Pi_h \boldsymbol{u}_h) = \int_\Omega \boldsymbol{f} \times \boldsymbol{x} \, \mathrm{d}\boldsymbol{x}.$$

*Proof.* Taking $\boldsymbol{v}_h = \chi(\boldsymbol{e}_i), \chi(\tilde{\boldsymbol{e}}_i)$ with $\tilde{\boldsymbol{e}}_i := \boldsymbol{x} \times \boldsymbol{e}_i$ in (2.12), by Assumption 2 one obtains

$$(\partial_t(\Pi_h \boldsymbol{u}_h), \boldsymbol{e}_i) + \nu a(\boldsymbol{u}_h, \boldsymbol{e}_i) + c_h(\boldsymbol{u}_h, \boldsymbol{u}_h, \boldsymbol{e}_i) - b(\boldsymbol{e}_i, p_h) = (\boldsymbol{f}, \boldsymbol{e}_i),$$

and

$$(\partial_t(\Pi_h \boldsymbol{u}_h), \tilde{\boldsymbol{e}}_i) + \nu a(\boldsymbol{u}_h, \tilde{\boldsymbol{e}}_i) + c_h(\boldsymbol{u}_h, \boldsymbol{u}_h, \tilde{\boldsymbol{e}}_i) - b(\tilde{\boldsymbol{e}}_i, p_h) = (\boldsymbol{f}, \tilde{\boldsymbol{e}}_i) = (\boldsymbol{f} \times \boldsymbol{x}, \boldsymbol{e}_i),$$

where in the last inequality we also apply (2.18). Since $\Delta \boldsymbol{e}_i = \Delta \tilde{\boldsymbol{e}}_i = \boldsymbol{0}$ and $\nabla \cdot \boldsymbol{e}_i = \nabla \cdot \tilde{\boldsymbol{e}}_i = 0$, it suffices to prove that

$$c_h(\boldsymbol{u}_h, \boldsymbol{u}_h, \boldsymbol{e}_i) = 0 \quad \text{and} \quad c_h(\boldsymbol{u}_h, \boldsymbol{u}_h, \tilde{\boldsymbol{e}}_i) = 0.$$

By $\nabla \boldsymbol{e}_i = \boldsymbol{0}$, Lemma 2 and (2.17) imply that

$$c_h(\boldsymbol{u}_h, \boldsymbol{u}_h, \boldsymbol{e}_i) = -c_h(\boldsymbol{u}_h, \boldsymbol{e}_i, \boldsymbol{u}_h) = -c(\Pi_h \boldsymbol{u}_h, \boldsymbol{e}_i, \Pi_h \boldsymbol{u}_h) = 0,$$

and

$$c_h(\boldsymbol{u}_h, \boldsymbol{u}_h, \tilde{\boldsymbol{e}}_i) = -c(\Pi_h \boldsymbol{u}_h, \tilde{\boldsymbol{e}}_i, \Pi_h \boldsymbol{u}_h) = (\Pi_h \boldsymbol{u}_h \times \Pi_h \boldsymbol{u}_h, \boldsymbol{e}_i) = 0,$$

together with (2.19). Thus we complete the proof. □

For the case $\nu = 0$ (the Euler equations), if we apply the no-penetration boundary condition ($\boldsymbol{u}\cdot\boldsymbol{n} = 0$ on $J\times\Gamma$), the skew-symmetry of $c_h$ still holds by Lemma 1. Thus Theorem 1 implies that the method (2.12) conserves a discrete energy for $\nu = 0$ and $\boldsymbol{f} = \boldsymbol{0}$, with only no-penetration boundary condition strongly imposed. Theorem 2 implies that (2.12) conserves linear momentum and angular momentum (of $\Pi_h\boldsymbol{u}_h$) for $\boldsymbol{f}$ with zero momentum and zero angular momentum under Assumption 2, respectively.

**Remark 3** (Momentum analysis for the rotational form (2.11))**.** We use linear momentum as an example. By equation (8) of [12], we have

$$c_{\mathrm{rot}}(\boldsymbol{u}_h,\boldsymbol{u}_h,\boldsymbol{v}_h) = c(\Pi_h\boldsymbol{u}_h,\boldsymbol{u}_h,\Pi_h\boldsymbol{v}_h) - c(\Pi_h\boldsymbol{v}_h,\boldsymbol{u}_h,\Pi_h\boldsymbol{u}_h).$$

Then taking $\boldsymbol{v}_h = \chi(\boldsymbol{e}_i)$ gives

$$\begin{aligned} c_{\mathrm{rot}}(\boldsymbol{u}_h,\boldsymbol{u}_h,\boldsymbol{e}_i) &= c(\Pi_h\boldsymbol{u}_h,\boldsymbol{u}_h,\boldsymbol{e}_i) - c(\boldsymbol{e}_i,\boldsymbol{u}_h,\Pi_h\boldsymbol{u}_h)\\ &= -c(\Pi_h\boldsymbol{u}_h,\boldsymbol{e}_i,\boldsymbol{u}_h) - c(\boldsymbol{e}_i,\boldsymbol{u}_h,\Pi_h\boldsymbol{u}_h) \quad \text{(by Lem. 1)}\\ &= -c(\boldsymbol{e}_i,\boldsymbol{u}_h,\Pi_h\boldsymbol{u}_h) \neq 0. \end{aligned}$$

Thus linear momentum is not preserved by $c_{\mathrm{rot}}$.

## 3. A pressure-robust and Re-semi-robust error estimate

Let $\boldsymbol{u}$ solve (2.9). We assume $\Delta\boldsymbol{u}\in L^2\big(J;\boldsymbol{L}^2(\Omega)\big)$. Multiplying $\Pi_h\boldsymbol{v}_h\in\Pi_h\boldsymbol{V}_h^0$ on the two sides of (1.1a) and integrating over $\Omega$, one arrives at

$$(\partial_t\boldsymbol{u},\Pi_h\boldsymbol{v}_h) - \nu(\Delta\boldsymbol{u},\Pi_h\boldsymbol{v}_h) + c(\boldsymbol{u},\boldsymbol{u},\Pi_h\boldsymbol{v}_h) = (\boldsymbol{f},\Pi_h\boldsymbol{v}_h) \quad \forall\boldsymbol{v}_h\in\boldsymbol{V}_h^0, \tag{3.1}$$

where the term $(\nabla p,\Pi_h\boldsymbol{v}_h)$ has been removed since $\nabla\cdot\Pi_h\boldsymbol{v}_h\equiv 0$.

Subtracting (2.12) from (3.1) we get the error equation

$$\begin{aligned} (\partial_t(\boldsymbol{u}-\Pi_h\boldsymbol{u}_h),\Pi_h\boldsymbol{v}_h) + \alpha\big(\partial_t(\Pi_h^{\mathrm{R}}\boldsymbol{u}_h),\Pi_h^{\mathrm{R}}\boldsymbol{v}_h\big) + \nu(\nabla(\boldsymbol{u}-\boldsymbol{u}_h),\nabla\boldsymbol{v}_h) + c(\boldsymbol{u},\boldsymbol{u},\Pi_h\boldsymbol{v}_h)\\ - c_h(\boldsymbol{u}_h,\boldsymbol{u}_h,\boldsymbol{v}_h) = \delta_h(\boldsymbol{u},\boldsymbol{v}_h) \quad \forall\boldsymbol{v}_h\in\boldsymbol{V}_h^0, \end{aligned} \tag{3.2}$$

where

$$\delta_h(\boldsymbol{u},\boldsymbol{v}_h) := \nu(\Delta\boldsymbol{u},\Pi_h\boldsymbol{v}_h) + \nu(\nabla\boldsymbol{u},\nabla\boldsymbol{v}_h) = -\nu(\Delta\boldsymbol{u},(1-\Pi_h)\boldsymbol{v}_h)$$

is the consistency error from the diffusion term [43, 45].

Denote by $\Pi_h^{\mathrm{S}}:\boldsymbol{V}^0\to\boldsymbol{V}_h^0$ the Stokes projection which satisfies

$$\big(\nabla\big(\boldsymbol{v}-\Pi_h^{\mathrm{S}}\boldsymbol{v}\big),\nabla\boldsymbol{w}_h\big) = 0 \quad \forall\boldsymbol{v}\in\boldsymbol{V}^0,\boldsymbol{w}_h\in\boldsymbol{V}_h^0. \tag{3.3}$$

**Assumption 3.** *For any $\boldsymbol{v}\in\boldsymbol{V}^0\cap\boldsymbol{W}^{1,\infty}(\Omega)$, there exists a positive constant $C_{\mathrm{inf}}$ which is independent of $h$ such that*

$$\big\|\nabla\Pi_h^{\mathrm{S}}\boldsymbol{v}\big\|_\infty \le C_{\mathrm{inf}}\|\nabla\boldsymbol{v}\|_\infty. \tag{3.4}$$

This estimate is proven in Theorem 13 from [26] under the assumptions that $\Omega$ is convex and $\mathcal{T}_h$ is quasi-uniform.

Split the error $\boldsymbol{u}-\boldsymbol{u}_h$ as

$$\boldsymbol{e}_h := \boldsymbol{u}-\boldsymbol{u}_h = \boldsymbol{u}-\Pi_h^{\mathrm{S}}\boldsymbol{u} + \Pi_h^{\mathrm{S}}\boldsymbol{u}-\boldsymbol{u}_h = \boldsymbol{\eta}+\boldsymbol{\phi}_h. \tag{3.5}$$

We also define $\boldsymbol{\eta}_\pi := \boldsymbol{u}-\Pi_h\Pi_h^{\mathrm{S}}\boldsymbol{u}$, $\boldsymbol{\eta}_\pi^1 := \boldsymbol{u}-\Pi_h^1\Pi_h^{\mathrm{S}}\boldsymbol{u}$ and $\boldsymbol{\eta}_\pi^{\mathrm{R}} := -\Pi_h^{\mathrm{R}}\Pi_h^{\mathrm{S}}\boldsymbol{u}$. Note that $\boldsymbol{\eta}_\pi^{\mathrm{R}}$ is a function in $\boldsymbol{X}_h$.

Next, we introduce the dual norm $\|\cdot\|_{(\boldsymbol{V}_h^0)'}$ for any linear functional $L$ on $\boldsymbol{V}_h^0$:

$$\|L\|_{(\boldsymbol{V}_h^0)'} := \sup_{\boldsymbol{v}_h \in \boldsymbol{V}_h^0 \setminus \{\boldsymbol{0}\}} \frac{L(\boldsymbol{v}_h)}{\|\nabla \boldsymbol{v}_h\|},$$

or for any $\boldsymbol{g} \in \boldsymbol{L}^2(\Omega)$:

$$\|\boldsymbol{g}\|_{(\boldsymbol{V}_h^0)'} := \sup_{\boldsymbol{v}_h \in \boldsymbol{V}_h^0 \setminus \{\boldsymbol{0}\}} \frac{(\boldsymbol{g}, \boldsymbol{v}_h)}{\|\nabla \boldsymbol{v}_h\|}.$$

We also define a mesh-dependent norm $|||\cdot|||_*$ on $\boldsymbol{X}_h$ by

$$|||\boldsymbol{w}|||_*^2 := \sum_{K \in \mathcal{T}_h} h_K^{-2} \|\boldsymbol{w}\|_K^2. \tag{3.6}$$

The following two inequalities will be used to estimate the nonlinear terms.

**Lemma 3.** *Let $C_{\mathrm{inv}}$ denote a generic constant in inverse inequalities. Then one has*

$$c(\boldsymbol{z}, \boldsymbol{v}, \boldsymbol{w}) \le C_{\mathrm{inv}} \|\boldsymbol{z}\|_\infty \|\boldsymbol{v}\| |||\boldsymbol{w}|||_* \tag{3.7}$$

*for $(\widetilde{\boldsymbol{z}}, \widetilde{\boldsymbol{v}}, \widetilde{\boldsymbol{w}}) \in \boldsymbol{L}^\infty(\Omega) \times \boldsymbol{V}_h \times \boldsymbol{X}_h$ and*

$$c\big(\widetilde{\boldsymbol{z}}, \widetilde{\boldsymbol{v}}, \Pi_h^{\mathrm{R}} \widetilde{\boldsymbol{w}}\big) \le C_{\mathrm{inv}} C_{\mathrm{R},\infty} \|\widetilde{\boldsymbol{z}}\| |||\widetilde{\boldsymbol{v}}||| |\widetilde{\boldsymbol{w}}|_{1,\infty} \tag{3.8}$$

*for $(\widetilde{\boldsymbol{z}}, \widetilde{\boldsymbol{v}}, \widetilde{\boldsymbol{w}}) \in \boldsymbol{L}^2(\Omega) \times \boldsymbol{V}_h \times \boldsymbol{V}_h^0$.*

*Proof.* It follows from the Schwarz's inequality and the inverse inequality that

$$\begin{aligned} c(\boldsymbol{z}, \boldsymbol{v}, \boldsymbol{w}) &= \sum_{K \in \mathcal{T}_h} ((\boldsymbol{z} \cdot \nabla)\boldsymbol{v}, \boldsymbol{w})_K \le \|\boldsymbol{z}\|_\infty \sum_{K \in \mathcal{T}_h} \|\nabla \boldsymbol{v}\|_K \|\boldsymbol{w}\|_K \\ &\le \|\boldsymbol{z}\|_\infty \left( \sum_{K \in \mathcal{T}_h} h_K^2 \|\nabla \boldsymbol{v}\|_K^2 \right)^{1/2} \left( \sum_{K \in \mathcal{T}_h} h_K^{-2} \|\boldsymbol{w}\|_K^2 \right)^{1/2} \\ &\le C_{\mathrm{inv}} \|\boldsymbol{z}\|_\infty \|\boldsymbol{v}\| |||\boldsymbol{w}|||_*. \end{aligned}$$

For the second inequality, from (2.8) similarly we have

$$\begin{aligned} c\big(\widetilde{\boldsymbol{z}}, \widetilde{\boldsymbol{v}}, \Pi_h^{\mathrm{R}} \widetilde{\boldsymbol{w}}\big) &= \sum_{K \in \mathcal{T}_h} \big((\widetilde{\boldsymbol{z}} \cdot \nabla)\widetilde{\boldsymbol{v}}, \Pi_h^{\mathrm{R}} \widetilde{\boldsymbol{w}}\big)_K \le \sum_{K \in \mathcal{T}_h} \|\widetilde{\boldsymbol{z}}\|_K \|\nabla \widetilde{\boldsymbol{v}}\|_K \big\|\Pi_h^{\mathrm{R}} \widetilde{\boldsymbol{w}}\big\|_{\infty,K} \\ &\le \sum_{K \in \mathcal{T}_h} \|\widetilde{\boldsymbol{z}}\|_K h_K \|\nabla \widetilde{\boldsymbol{v}}\|_K h_K^{-1} \big\|\Pi_h^{\mathrm{R}} \widetilde{\boldsymbol{w}}\big\|_{\infty,K} \\ &\le C_{\mathrm{inv}} C_{\mathrm{R},\infty} \sum_{K \in \mathcal{T}_h} \|\widetilde{\boldsymbol{z}}\|_K \|\widetilde{\boldsymbol{v}}\|_K |\widetilde{\boldsymbol{w}}|_{1,\infty,K} \le C_{\mathrm{inv}} C_{\mathrm{R},\infty} \|\widetilde{\boldsymbol{z}}\| |||\widetilde{\boldsymbol{v}}||| |\widetilde{\boldsymbol{w}}|_{1,\infty}. \end{aligned}$$

This completes the proof. □

**Theorem 3.** *Let $\boldsymbol{u}$ be the solution of (2.9) and $\boldsymbol{u}_h$ be the solution of (2.12). Under Assumptions 1, 3, and the assumptions that $\boldsymbol{u} \in L^2\big(J; \boldsymbol{W}^{1,\infty}(\Omega)\big) \cap L^4\big(J; \boldsymbol{H}^1(\Omega)\big)$, $\boldsymbol{u}_t \in L^2\big(J; \boldsymbol{L}^2(\Omega)\big)$, $\Delta \boldsymbol{u} \in L^2\big(J; \boldsymbol{L}^2(\Omega)\big)$, and $\boldsymbol{u}_h^0 = \Pi_h^{\mathrm{S}} \boldsymbol{u}^0$, with $C$ independent of $h$ and $\nu$ the following estimate holds:*

$$E_d(\boldsymbol{e}_h(T)) + \frac{\nu}{2} \int_0^T \|\nabla \boldsymbol{e}_h\|^2 \,\mathrm{d}t \le \Big( \|\boldsymbol{\eta}_\pi(T)\|^2 + \alpha \big\|\boldsymbol{\eta}_\pi^{\mathrm{R}}(T)\big\|^2 \Big) + \nu \int_0^T \|\nabla \boldsymbol{\eta}\|^2 \,\mathrm{d}t$$

$$+ e^{G(\boldsymbol{u},T)} \int_0^T \left\{ T\Big( \|\partial_t \boldsymbol{\eta}_\pi\|^2 + \alpha \big\|\partial_t \boldsymbol{\eta}_\pi^{\mathrm{R}}\big\|^2 \Big) + \nu \|\Delta \boldsymbol{u} \circ (1-\Pi_h)\|^2_{(\boldsymbol{V}_h^0)'} \right.$$
$$\left. + C\|\boldsymbol{u}\|_{1,\infty} \Big( \|\boldsymbol{\eta}_\pi\|^2 + \big\|\nabla \boldsymbol{\eta}_\pi^1\big\|^2 + |||\boldsymbol{\eta}_\pi^{\mathrm{R}}|||_*^2 \Big) \right\} \mathrm{d}t, \tag{3.9}$$

*where*

$$G(\boldsymbol{u},T) = 1 + \int_0^T \Big\{ (1+C_{\mathrm{inv}})\|\boldsymbol{u}\|_\infty + 3C_{\mathrm{inf}}(C_{1,\infty} + C_{\mathrm{inv}} C_{\mathrm{R},\infty})|\boldsymbol{u}|_{1,\infty}$$
$$+ \alpha^{-1}(C_{\mathrm{inv}}\|\boldsymbol{u}\|_\infty + 2C_{\mathrm{inv}} C_{\mathrm{R},\infty} C_{\mathrm{inf}} |\boldsymbol{u}|_{1,\infty}) \Big\} \mathrm{d}t. \tag{3.10}$$

*Proof.* Substituting (3.5) into (3.2) and taking $\boldsymbol{v}_h = \boldsymbol{\phi}_h$ give that

$$\frac{\mathrm{d}}{\mathrm{d}t} E_d(\boldsymbol{\phi}_h) + \nu \|\nabla \boldsymbol{\phi}_h\|^2 = -(\partial_t \boldsymbol{\eta}_\pi, \Pi_h \boldsymbol{\phi}_h) - \alpha\big(\partial_t \boldsymbol{\eta}_\pi^{\mathrm{R}}, \Pi_h^{\mathrm{R}} \boldsymbol{\phi}_h\big) \underbrace{- \nu(\nabla \boldsymbol{\eta}, \nabla \boldsymbol{\phi}_h)}_{=0 \text{ by } (3.3)}$$
$$\underbrace{-c(\boldsymbol{u},\boldsymbol{u},\Pi_h\boldsymbol{\phi}_h) + c_h(\boldsymbol{u}_h,\boldsymbol{u}_h,\boldsymbol{\phi}_h)}_{\mathcal{NL}} + \delta_h(\boldsymbol{u},\boldsymbol{\phi}_h). \tag{3.11}$$

Let us estimate each term in (3.11). For the evolutionary term we have

$$\big|(\partial_t \boldsymbol{\eta}_\pi, \Pi_h \boldsymbol{\phi}_h) + \alpha\big(\partial_t \boldsymbol{\eta}_\pi^{\mathrm{R}}, \Pi_h^{\mathrm{R}} \boldsymbol{\phi}_h\big)\big| \le \frac{T}{2}\Big( \|\partial_t \boldsymbol{\eta}_\pi\|^2 + \alpha \big\|\partial_t \boldsymbol{\eta}_\pi^{\mathrm{R}}\big\|^2 \Big) + \frac{1}{T} E_d(\boldsymbol{\phi}_h). \tag{3.12}$$

For $\delta_h$ term the estimate can be found in [43]:

$$|\delta_h(\boldsymbol{u},\boldsymbol{\phi}_h)| \le \frac{1}{2}\nu \|\Delta \boldsymbol{u} \circ (1-\Pi_h)\|^2_{(\boldsymbol{V}_h^0)'} + \frac{1}{2}\nu \|\nabla \boldsymbol{\phi}_h\|^2. \tag{3.13}$$

Now, let us estimate the convective terms. We use a similar decomposition with [49, 55]:

$$\begin{aligned} -\mathcal{NL} &= c\big(\boldsymbol{u}, \boldsymbol{\eta}_\pi^1, \Pi_h \boldsymbol{\phi}_h\big) + c\big(\boldsymbol{u}, \Pi_h^1 \Pi_h^{\mathrm{S}} \boldsymbol{u}, \Pi_h \boldsymbol{\phi}_h\big) - c_h(\boldsymbol{u}_h, \boldsymbol{u}_h, \boldsymbol{\phi}_h) \\ &= c\big(\boldsymbol{u}, \boldsymbol{\eta}_\pi^1, \Pi_h \boldsymbol{\phi}_h\big) + c\big(\boldsymbol{u}, \Pi_h^1 \Pi_h^{\mathrm{S}} \boldsymbol{u}, \Pi_h \boldsymbol{\phi}_h\big) - c_h\big(\Pi_h^{\mathrm{S}} \boldsymbol{u}, \Pi_h^{\mathrm{S}} \boldsymbol{u}, \boldsymbol{\phi}_h\big) + c_h\big(\Pi_h^{\mathrm{S}} \boldsymbol{u}, \Pi_h^{\mathrm{S}} \boldsymbol{u}, \boldsymbol{\phi}_h\big) - c_h(\boldsymbol{u}_h, \boldsymbol{u}_h, \boldsymbol{\phi}_h). \end{aligned}$$

Recall $\boldsymbol{\eta}_\pi^{\mathrm{R}} = -\Pi_h^{\mathrm{R}} \Pi_h^{\mathrm{S}} \boldsymbol{u}$. We have

$$\begin{aligned} c\big(\boldsymbol{u}, \Pi_h^1 \Pi_h^{\mathrm{S}} \boldsymbol{u}, \Pi_h \boldsymbol{\phi}_h\big) - c_h\big(\Pi_h^{\mathrm{S}} \boldsymbol{u}, \Pi_h^{\mathrm{S}} \boldsymbol{u}, \boldsymbol{\phi}_h\big) &= c\big(\boldsymbol{u}, \Pi_h^1 \Pi_h^{\mathrm{S}} \boldsymbol{u}, \Pi_h \boldsymbol{\phi}_h\big) - c\big(\Pi_h \Pi_h^{\mathrm{S}} \boldsymbol{u}, \Pi_h^1 \Pi_h^{\mathrm{S}} \boldsymbol{u}, \Pi_h \boldsymbol{\phi}_h\big) \\ &\quad + c\big(\Pi_h \Pi_h^{\mathrm{S}} \boldsymbol{u}, \Pi_h^1 \boldsymbol{\phi}_h, \Pi_h^{\mathrm{R}} \Pi_h^{\mathrm{S}} \boldsymbol{u}\big) \\ &= c\big(\boldsymbol{\eta}_\pi, \Pi_h^1 \Pi_h^{\mathrm{S}} \boldsymbol{u}, \Pi_h \boldsymbol{\phi}_h\big) + c\big(\Pi_h \Pi_h^{\mathrm{S}} \boldsymbol{u}, \Pi_h^1 \boldsymbol{\phi}_h, \Pi_h^{\mathrm{R}} \Pi_h^{\mathrm{S}} \boldsymbol{u}\big) \\ &\quad - c\big(\boldsymbol{u}, \Pi_h^1 \boldsymbol{\phi}_h, \Pi_h^{\mathrm{R}} \Pi_h^{\mathrm{S}} \boldsymbol{u}\big) + c\big(\boldsymbol{u}, \Pi_h^1 \boldsymbol{\phi}_h, \Pi_h^{\mathrm{R}} \Pi_h^{\mathrm{S}} \boldsymbol{u}\big) \\ &= c\big(\boldsymbol{\eta}_\pi, \Pi_h^1 \Pi_h^{\mathrm{S}} \boldsymbol{u}, \Pi_h \boldsymbol{\phi}_h\big) - c\big(\boldsymbol{\eta}_\pi, \Pi_h^1 \boldsymbol{\phi}_h, \Pi_h^{\mathrm{R}} \Pi_h^{\mathrm{S}} \boldsymbol{u}\big) - c\big(\boldsymbol{u}, \Pi_h^1 \boldsymbol{\phi}_h, \boldsymbol{\eta}_\pi^{\mathrm{R}}\big) \end{aligned}$$

and

$$\begin{aligned} c_h\big(\Pi_h^{\mathrm{S}} \boldsymbol{u}, \Pi_h^{\mathrm{S}} \boldsymbol{u}, \boldsymbol{\phi}_h\big) - c_h(\boldsymbol{u}_h, \boldsymbol{u}_h, \boldsymbol{\phi}_h) &= c_h\big(\Pi_h^{\mathrm{S}} \boldsymbol{u}, \Pi_h^{\mathrm{S}} \boldsymbol{u}, \boldsymbol{\phi}_h\big) - c_h\big(\boldsymbol{u}_h, \Pi_h^{\mathrm{S}} \boldsymbol{u}, \boldsymbol{\phi}_h\big) \\ &\quad + c_h\big(\boldsymbol{u}_h, \Pi_h^{\mathrm{S}} \boldsymbol{u}, \boldsymbol{\phi}_h\big) - c_h(\boldsymbol{u}_h, \boldsymbol{u}_h, \boldsymbol{\phi}_h) \\ &= c_h\big(\boldsymbol{\phi}_h, \Pi_h^{\mathrm{S}} \boldsymbol{u}, \boldsymbol{\phi}_h\big) + c_h(\boldsymbol{u}_h, \boldsymbol{\phi}_h, \boldsymbol{\phi}_h) = c_h\big(\boldsymbol{\phi}_h, \Pi_h^{\mathrm{S}} \boldsymbol{u}, \boldsymbol{\phi}_h\big). \end{aligned}$$

It follows from the Schwarz's inequality, Young's inequality, Lemma 3, Assumptions 1, and 3 that

$$\big|c\big(\boldsymbol{u}, \boldsymbol{\eta}_\pi^1, \Pi_h \boldsymbol{\phi}_h\big)\big| \le \|\boldsymbol{u}\|_\infty \big\|\nabla \boldsymbol{\eta}_\pi^1\big\| \|\Pi_h \boldsymbol{\phi}_h\| \le \|\boldsymbol{u}\|_\infty \left( \frac{1}{2}\big\|\nabla \boldsymbol{\eta}_\pi^1\big\|^2 + \frac{1}{2}\|\Pi_h \boldsymbol{\phi}_h\|^2 \right),$$

$$
\begin{aligned}
\left|c(\boldsymbol{\eta}_\pi, \Pi_h^1\Pi_h^{\mathrm{S}}\boldsymbol{u}, \Pi_h\boldsymbol{\phi}_h)\right| &\le C_{1,\infty}C_{\inf}|\boldsymbol{u}|_{1,\infty}\left(\frac{1}{2}\|\boldsymbol{\eta}_\pi\|^2 + \frac{1}{2}\|\Pi_h\boldsymbol{\phi}_h\|^2\right),\\
\left|c(\boldsymbol{\eta}_\pi, \Pi_h^1\boldsymbol{\phi}_h, \Pi_h^{\mathrm{R}}\Pi_h^{\mathrm{S}}\boldsymbol{u})\right| &\le C_{\mathrm{inv}}C_{\mathrm{R},\infty}\left|\Pi_h^{\mathrm{S}}\boldsymbol{u}\right|_{1,\infty}\left(\frac{1}{2}\|\boldsymbol{\eta}_\pi\|^2 + \frac{1}{2}\left\|\Pi_h^1\boldsymbol{\phi}_h\right\|^2\right)\\
&\le C_{\mathrm{inv}}C_{\mathrm{R},\infty}C_{\inf}|\boldsymbol{u}|_{1,\infty}\left(\frac{1}{2}\|\boldsymbol{\eta}_\pi\|^2 + \frac{1}{2}\left\|\Pi_h^1\boldsymbol{\phi}_h\right\|^2\right),\\
\left|c(\boldsymbol{u}, \Pi_h^1\boldsymbol{\phi}_h, \boldsymbol{\eta}_\pi^{\mathrm{R}})\right| &\le C_{\mathrm{inv}}\|\boldsymbol{u}\|_\infty\left(\frac{1}{2}\left\|\Pi_h^1\boldsymbol{\phi}_h\right\|^2 + \frac{1}{2}|||\boldsymbol{\eta}_\pi^{\mathrm{R}}|||_*^2\right),
\end{aligned}
$$

and

$$
\begin{aligned}
\left|c_h(\boldsymbol{\phi}_h, \Pi_h^{\mathrm{S}}\boldsymbol{u}, \boldsymbol{\phi}_h)\right| &= \left|c(\Pi_h\boldsymbol{\phi}_h, \Pi_h^1\Pi_h^{\mathrm{S}}\boldsymbol{u}, \Pi_h\boldsymbol{\phi}_h) - c(\Pi_h\boldsymbol{\phi}_h, \Pi_h^1\boldsymbol{\phi}_h, \Pi_h^{\mathrm{R}}\Pi_h^{\mathrm{S}}\boldsymbol{u})\right|\\
&\le C_{1,\infty}C_{\inf}|\boldsymbol{u}|_{1,\infty}\|\Pi_h\boldsymbol{\phi}_h\|^2 + C_{\mathrm{inv}}C_{\mathrm{R},\infty}C_{\inf}|\boldsymbol{u}|_{1,\infty}\left(\frac{1}{2}\|\Pi_h\boldsymbol{\phi}_h\|^2 + \frac{1}{2}\left\|\Pi_h^1\boldsymbol{\phi}_h\right\|^2\right).
\end{aligned}
$$

Based on the above estimates for the nonlinear terms, one can obtain that

$$
|\mathcal{NL}| \le C\|\boldsymbol{u}\|_{1,\infty}\left(\|\boldsymbol{\eta}_\pi\|^2 + \left\|\nabla\boldsymbol{\eta}_\pi^1\right\|^2 + |||\boldsymbol{\eta}_\pi^{\mathrm{R}}|||_*^2\right) + \frac{1}{2}\mathcal{C}_1\|\Pi_h\boldsymbol{\phi}_h\|^2 + \frac{1}{2}\mathcal{C}_2\left\|\Pi_h^1\boldsymbol{\phi}_h\right\|^2, \tag{3.14}
$$

where

$$
\mathcal{C}_1 := \|\boldsymbol{u}\|_\infty + C_{\inf}(3C_{1,\infty} + C_{\mathrm{inv}}C_{\mathrm{R},\infty})|\boldsymbol{u}|_{1,\infty}, \quad \mathcal{C}_2 := C_{\mathrm{inv}}\|\boldsymbol{u}\|_\infty + 2C_{\mathrm{inv}}C_{\mathrm{R},\infty}C_{\inf}|\boldsymbol{u}|_{1,\infty}.
$$

Then substituting (3.12)–(3.14) into (3.11) provides

$$
\begin{aligned}
\frac{\mathrm{d}}{\mathrm{d}t}E_d(\boldsymbol{\phi}_h) + \frac{\nu}{2}\|\nabla\boldsymbol{\phi}_h\|^2 \le{}& \frac{T}{2}\left(\|\partial_t\boldsymbol{\eta}_\pi\|^2 + \alpha\left\|\partial_t\boldsymbol{\eta}_\pi^{\mathrm{R}}\right\|^2\right) + \frac{1}{T}E_d(\boldsymbol{\phi}_h) + \frac{1}{2}\nu\|\Delta\boldsymbol{u}\circ(1-\Pi_h)\|_{(\boldsymbol{V}_h^0)'}^2\\
&+ C\|\boldsymbol{u}\|_{1,\infty}\left(\|\boldsymbol{\eta}_\pi\|^2 + \left\|\nabla\boldsymbol{\eta}_\pi^1\right\|^2 + |||\boldsymbol{\eta}_\pi^{\mathrm{R}}|||_*^2\right) + \frac{1}{2}\mathcal{C}_1\|\Pi_h\boldsymbol{\phi}_h\|^2 + \frac{1}{2}\mathcal{C}_2\left\|\Pi_h^1\boldsymbol{\phi}_h\right\|^2.
\end{aligned} \tag{3.15}
$$

Note that $\|\Pi_h\boldsymbol{\phi}_h\|^2 \le 2E_d(\boldsymbol{\phi}_h)$ and $\left\|\Pi_h^1\boldsymbol{\phi}_h\right\|^2 \le (2+2/\alpha)E_d(\boldsymbol{\phi}_h)$ by Lemma 3 of [9] with "$\xi$"$=\Pi_h^1\boldsymbol{\phi}_h$ and "$\eta$"$=\Pi_h^{\mathrm{R}}\boldsymbol{\phi}_h$ therein. Integrating over $J$, and applying the fact $\boldsymbol{u}_h(0) = \Pi_h^{\mathrm{S}}\boldsymbol{u}(0)$ and the Gronwall inequality, we can get

$$
\begin{aligned}
E_d(\boldsymbol{\phi}_h(T)) + \frac{\nu}{2}\int_0^T\|\nabla\boldsymbol{\phi}_h\|^2\,\mathrm{d}t \le e^{G(\boldsymbol{u},T)}\int_0^T\Bigg\{&\frac{T}{2}\left(\|\partial_t\boldsymbol{\eta}_\pi\|^2 + \alpha\left\|\partial_t\boldsymbol{\eta}_\pi^{\mathrm{R}}\right\|^2\right) + \frac{\nu}{2}\|\Delta\boldsymbol{u}\circ(1-\Pi_h)\|_{(\boldsymbol{V}_h^0)'}^2\\
&+ C\|\boldsymbol{u}\|_{1,\infty}\left(\|\boldsymbol{\eta}_\pi\|^2 + \left\|\nabla\boldsymbol{\eta}_\pi^1\right\|^2 + |||\boldsymbol{\eta}_\pi^{\mathrm{R}}|||_*^2\right)\Bigg\}\,\mathrm{d}t.
\end{aligned}
$$

Then (3.9) follows immediately from a combination of the above inequality and the Young's inequality. □

**Remark 4** (The choice of $\alpha$)**.** For the error estimate (3.9), on the one hand, a larger $\alpha$ results in a smaller Gronwall constant $G(\boldsymbol{u}, T)$, but on the other hand, the existence of the terms $\alpha\left\|\boldsymbol{\eta}_\pi^{\mathrm{R}}(T)\right\|^2$ and $\alpha\left\|\partial_t\boldsymbol{\eta}_\pi^{\mathrm{R}}\right\|^2$ does not allow a too large $\alpha$. The optimal choice of $\alpha$ is still an open problem. By observing the Gronwall constant, it seems that $\alpha \ll 1$ is not a good choice since the $\alpha$-related part can dominate the other part with such an $\alpha$. Some numerical study on $\alpha$ will be given in Section 5.

## 4. The reconstruction operators for a class of simplicial non-divergence-free elements

In this section, we focus on a class of simplicial locally mass-conserving elements which satisfy the inf-sup condition (2.2), and give the corresponding divergence-free reconstruction operators. First, let us recall their

TABLE 1. Local velocity spaces on an element $K$. For $k = 1$, one usually calls it as Bernardi–Raugel space.

| Order | Dimension | Local space |
|---|---|---|
| $k = 1$ | 2D/3D | $\boldsymbol{\mathcal{P}}_k^{\mathrm{b}}(K) = [P_1(K)]^d \oplus \mathrm{span}\{\boldsymbol{b}_i, 1 \le i \le d+1\}$ |
| $k \ge 2$ | 2D | $\boldsymbol{\mathcal{P}}_k^{\mathrm{b}}(K) = \left[P_k(K) \oplus b_K \tilde{P}_{k-2}(K)\right]^2$ |
| $k = 2$ | 3D | $\boldsymbol{\mathcal{P}}_k^{\mathrm{b}}(K) = \left[P_2(K) \oplus b_K \tilde{P}_0(K)\right]^3 \oplus \mathrm{span}\{\boldsymbol{b}_i, 1 \le i \le 4\}$ |
| $k \ge 3$ | 3D | $\boldsymbol{\mathcal{P}}_k^{\mathrm{b}}(K) = \left[P_k(K) \oplus b_K \left(\tilde{P}_{k-2}(K) \oplus \tilde{P}_{k-3}(K)\right)\right]^3$ |

construction in [25], pp. 132–144, where the lowest order case is the well-known Bernardi–Raugel element [6]. Consider an arbitrary element $K$ with vertices $\boldsymbol{a}_i, 1 \le i \le d+1$. Denote by $F_i$ the face opposite to $\boldsymbol{a}_i$ and $\boldsymbol{n}_i$ the unit outward normal vector corresponding to $F_i, 1 \le i \le d+1$. Further, $\lambda_i, 1 \le i \le d+1$, denote the corresponding barycentric coordinates. Then the (normal-weighted) face bubbles are defined by

$$\boldsymbol{b}_i := \left(\prod_{1 \le j \le d+1; j \ne i} \lambda_j\right) \boldsymbol{n}_i, 1 \le i \le d+1.$$

We also define

$$b_K := \prod_{1 \le j \le d+1} \lambda_j, \quad \text{and} \quad \tilde{P}_k(K) := \mathrm{span}\left\{\prod_{i=1}^{d} x_i^{k_i}, k_i \ge 0, 1 \le i \le d, \sum_{i=1}^{d} k_i = k\right\}.$$

Then the local finite element spaces for velocity on an element $K$ are defined as Table 1.

For $k$-th order velocity spaces, the matching pressure space is the space of discontinuous piecewise polynomials of degree no more than $k-1$, whatever the dimension is. In what follows, $\boldsymbol{V}_h$ will denote a velocity space of order $k$ mentioned above and $W_h$ is the corresponding pressure space. From Table 1 one can see there exists a space of bubble functions $\boldsymbol{V}_h^b \cong \boldsymbol{V}_h / \boldsymbol{P}_k$ such that $\boldsymbol{V}_h = \boldsymbol{P}_k \oplus \boldsymbol{V}_h^b$. For any $\boldsymbol{v}_h \in \boldsymbol{V}_h$, it is natural to split it into two parts:

$$\boldsymbol{v}_h = \boldsymbol{v}_h^1 + \boldsymbol{v}_h^b \text{ with } \boldsymbol{v}_h^1 \in \boldsymbol{P}_k, \boldsymbol{v}_h^b \in \boldsymbol{V}_h^b.$$

We consider a class of divergence-free reconstruction operators which were also discussed in Remark 4.2 of [43]. These operators are defined as follows. Let $I_h : \boldsymbol{C}^0(\bar{\Omega}) \to \boldsymbol{P}_k$ denote the standard interpolation operator to $\boldsymbol{P}_k$ (such as the interpolations defined in [25], pp. 99, 100). Then $\Pi_h^1$ is defined by

$$\Pi_h^1|_{\boldsymbol{V}_h} := I_h.$$

Let $\Pi_h^{\mathrm{RT}}$ be the common Raviart–Thomas interpolation of order $k-1$ [7]. The operator $\Pi_h^{\mathrm{R}}$ is defined by

$$\Pi_h^{\mathrm{R}}|_{\boldsymbol{V}_h} := \Pi_h^{\mathrm{RT}} \circ (1 - I_h). \tag{4.1}$$

Hence, for any $\boldsymbol{v}_h \in \boldsymbol{V}_h$ one has

$$\Pi_h \boldsymbol{v}_h = \Pi_h^1 \boldsymbol{v}_h + \Pi_h^{\mathrm{R}} \boldsymbol{v}_h = I_h \boldsymbol{v}_h + \Pi_h^{\mathrm{RT}}(\boldsymbol{v}_h - I_h \boldsymbol{v}_h). \tag{4.2}$$

At this time the space $\boldsymbol{X}_h$ could be chosen as

$$\boldsymbol{X}_h := \left\{\boldsymbol{v}_h \in \boldsymbol{H}(\mathrm{div}; \Omega) : \boldsymbol{v}_h|_K \in [P_k(K)]^d \text{ for all } K \in \mathcal{T}_h\right\}.$$

Clearly $\boldsymbol{X}_h$ and $W_h$ satisfy the relationship (2.3).

TABLE 2. Shape functions $\boldsymbol{\psi}_h$ for Bernardi–Raugel elements and $\Pi_h\boldsymbol{\psi}_h$ $(1 \le i \le d+1, 1 \le j \le d)$.

| $\boldsymbol{\psi}_h$ | $\lambda_i \boldsymbol{e}_j$ | $\boldsymbol{b}_i$ $(d=2)$ | $\boldsymbol{b}_i$ $(d=3)$ |
|---|---|---|---|
| $\Pi_h\boldsymbol{\psi}_h$ | $\lambda_i \boldsymbol{e}_j$ | $\frac{\lvert F_i\rvert}{6}\boldsymbol{q}^i_{\mathrm{RT}_0}$ | $\frac{\lvert F_i\rvert}{60}\boldsymbol{q}^i_{\mathrm{RT}_0}$ |

**Remark 5.** Under the setting above, for any $\boldsymbol{v}_h \in \boldsymbol{V}_h$ it holds that $\Pi_h\boldsymbol{v}_h = \boldsymbol{v}_h^1 + \Pi_h\boldsymbol{v}_h^b$. In other words, these reconstruction operators only change the bubble part of the elements. Thus the reconstruction is low-cost and has not changed much compared to the previous classical formulation. This is especially the case for the first order element and the second order element in two/three dimensions, since it is not hard to find that, for any $\boldsymbol{v}_h$ belonging to these spaces,

$$\Pi_h^1\boldsymbol{v}_h^b = 0 \Rightarrow \Pi_h\boldsymbol{v}_h^b = \Pi_h^{\mathrm{R}}\boldsymbol{v}_h^b = \Pi_h^{\mathrm{RT}}\boldsymbol{v}_h^b \Rightarrow \Pi_h\boldsymbol{v}_h = \boldsymbol{v}_h^1 + \Pi_h^{\mathrm{RT}}\boldsymbol{v}_h^b.$$

**Remark 6.** Another advantage of EMAPR is that it can lower the requirement of the quadrature rules dramatically. For classical discretizations, usually the convective term requires higher order quadrature rules. The use of bubble functions exacerbates the situations further since these functions are polynomials of higher degree. This limits the practical application of the simplicial locally mass-conserving elements. One can easily check that, to compute the convective term $c(\cdot,\cdot,\cdot)$ exactly, the quadrature rules with algebraic precision of degree 5 (8) are needed for two-dimensional (three-dimensional, respectively) Bernardi–Raugel element. However, in any dimensions for Bernardi–Raugel elements one only needs the quadrature rules with algebraic precision of degree 2 to compute $c_h(\cdot,\cdot,\cdot)$ exactly.

### 4.1. On the implementation of $\Pi_h$ for Bernardi–Raugel elements

This subsection discusses a detailed construction of $\Pi_h$ for Bernardi–Raugel elements. The reconstructed shape functions are explicitly provided, which can be used to assemble coefficient matrices for our methods in a standard way. Recall that $\boldsymbol{a}_i \in \mathbb{R}^d$ denotes the $i$-th vertex of $K$. On an element $K$, the shape functions for the lowest order Raviart–Thomas space have the form

$$\boldsymbol{q}^i_{\mathrm{RT}_0} := \frac{1}{d|T|}(\boldsymbol{x} - \boldsymbol{a}_i), \quad 0 \le i \le d+1,$$

which satisfy

$$\int_{F_j} \boldsymbol{q}^i_{\mathrm{RT}_0} \cdot \boldsymbol{n}_j \, ds = \delta_{ij} := \begin{cases} 1 & i = j, \\ 0 & i \ne j. \end{cases}$$

The relationship between the shape functions and reconstructed shape functions for the Bernardi–Raugel elements is listed in Table 2. Indeed, simple calculations give

$$\int_{F_i} \boldsymbol{b}_i \cdot \boldsymbol{n}_i \, \mathrm{d}\boldsymbol{x} = \begin{cases} |F_i|/6 & d = 2, \\ |F_i|/60 & d = 3. \end{cases}$$

Then Table 2 follows immediately from the definition of $\Pi_h$. One can use Table 2 and standard Raviart–Thomas basis functions to build the basis functions for $\Pi_h\boldsymbol{u}_h$ easily and locally. Then the matrix assembly of our method is very similar to that of the classical conforming methods, since the former also consists of volume integrals.

### 4.2. Error analysis

Next, let us analyze the properties of the reconstruction operators defined above. To analyze the convergence rates of EMAPR for the elements mentioned above, we shall assume that the true solution $\boldsymbol{u}(t)$ $(t \in J)$ is in

$\boldsymbol{H}^{\frac{3}{2}+\epsilon}(\Omega)$ with some $\epsilon > 0$. This assumption guarantees $\boldsymbol{u}(t) \in \boldsymbol{C}^0(\bar{\Omega})$ and thus $I_h\boldsymbol{u}$ is well-defined. We define $\boldsymbol{V}(\mathcal{T}_h) := \boldsymbol{C}^0(\bar{\Omega}) \cap \boldsymbol{H}^2(\mathcal{T}_h)$.

**Lemma 4.** *The operators $I_h$ and $\Pi_h^{\mathrm{RT}}$ satisfy*

$$\|\boldsymbol{v} - I_h\boldsymbol{v}\|_K + h_K\|\nabla(\boldsymbol{v} - I_h\boldsymbol{v})\|_K \le Ch_K^2|\boldsymbol{v}|_{2,K} \qquad \forall \boldsymbol{v} \in \boldsymbol{V}(\mathcal{T}_h), \tag{4.3}$$

$$\|\boldsymbol{v} - I_h\boldsymbol{v}\|_K + h_K\|\nabla(\boldsymbol{v} - I_h\boldsymbol{v})\|_K \le Ch_K^2|\boldsymbol{v} - I_h\boldsymbol{v}|_{2,K} \qquad \forall \boldsymbol{v} \in \boldsymbol{V}(\mathcal{T}_h), \tag{4.4}$$

$$\|\boldsymbol{v} - \Pi_h^{\mathrm{RT}}\boldsymbol{v}\|_K \le Ch_K\|\nabla\boldsymbol{v}\|_K \qquad \forall \boldsymbol{v} \in \boldsymbol{V}, \tag{4.5}$$

$$\|\Pi_h^{\mathrm{RT}}\boldsymbol{v}_h\|_{p,K} \le \|\boldsymbol{v}_h\|_{p,K}, \quad p = 2, \infty, \qquad \forall \boldsymbol{v}_h \in \boldsymbol{V}_h, \tag{4.6}$$

*and*

$$\left(\boldsymbol{v} - \Pi_h^{\mathrm{RT}}\boldsymbol{v}, \boldsymbol{w}\right)_K = 0 \quad \forall \boldsymbol{v} \in \boldsymbol{V}, \boldsymbol{w} \in [P_{k-2}(K)]^d \tag{4.7}$$

*for all $K \in \mathcal{T}_h$.*

*Proof.* We refer the readers to Theorem 4.4.4 of [8] and Propositions 2.5.1, 2.3.4 of [7] for (4.3), (4.5), and (4.7), respectively. Note that $I_h(\boldsymbol{v} - I_h\boldsymbol{v}) = \boldsymbol{0}$. Then replacing $\boldsymbol{v}$ with $\boldsymbol{v} - I_h\boldsymbol{v}$ in (4.3) gives (4.4).

Let us prove (4.6). We have

$$\|\boldsymbol{v}_h - \Pi_h^{\mathrm{RT}}\boldsymbol{v}_h\|_{p,K} \le Ch_K^{d/p-d/2}\|\boldsymbol{v}_h - \Pi_h^{\mathrm{RT}}\boldsymbol{v}_h\|_K \le Ch_K^{d/p-d/2+1}\|\nabla\boldsymbol{v}_h\|_K \le C\|\boldsymbol{v}_h\|_{p,K},$$

where we repeatedly use the local estimates in Lemma 4.5.3 of [8] and the interpolation error of $\Pi_h^{\mathrm{RT}}$ (4.5). Then (4.6) follows immediately from the triangle inequality. Note that (4.6) does not hold if $\boldsymbol{v}_h$ is an arbitrary function in $V$. □

**Lemma 5.** *The reconstruction operators defined by (4.2) satisfy (2.4)–(2.8) and (2.17).*

*Proof.* Equation (2.17) is clearly satisfied. Furthermore since (2.4) is implied in (2.5) due to $\nabla \cdot \Pi_h\boldsymbol{v}_h \in W_h$ for any $\boldsymbol{v}_h \in \boldsymbol{V}_h$ (see (2.3)), we only prove (2.5)–(2.8).

Denote by $P_h : L^2(\Omega) \to W_h$ the $L^2$ projection to $W_h$. Applying the commuting diagram property for $\Pi_h^{\mathrm{RT}}$ and $P_h$ (*e.g.*, see [7], Rem. 2.5.2) and (2.3) one can obtain

$$\begin{aligned} P_h\nabla \cdot \Pi_h\boldsymbol{v}_h &= \nabla \cdot \Pi_h\boldsymbol{v}_h = \nabla \cdot \Pi_h^1\boldsymbol{v}_h + \nabla \cdot \Pi_h^{\mathrm{RT}}(1 - \Pi_h^1)\boldsymbol{v}_h \\ &= \nabla \cdot \Pi_h^1\boldsymbol{v}_h + P_h\nabla \cdot (1 - \Pi_h^1)\boldsymbol{v}_h = P_h\nabla \cdot \boldsymbol{v}_h, \end{aligned}$$

which is exactly (2.5).

The proof of (2.6) is very similar to the analysis in [45]. In fact, for any $\boldsymbol{v}_h \in \boldsymbol{V}_h$, from (4.2) we have

$$\boldsymbol{v}_h - \Pi_h\boldsymbol{v}_h = (\boldsymbol{v}_h - I_h\boldsymbol{v}_h) - \Pi_h^{\mathrm{RT}}(\boldsymbol{v}_h - I_h\boldsymbol{v}_h), \tag{4.8}$$

which, together with (4.7), implies that

$$(\boldsymbol{v}_h - \Pi_h\boldsymbol{v}_h, \boldsymbol{w})_K = 0 \quad \forall \boldsymbol{w} \in [P_{k-2}(K)]^d, K \in \mathcal{T}_h. \tag{4.9}$$

On the other hand, from (4.8), (4.6), (4.3), and inverse inequalities, it follows that

$$\|\boldsymbol{v}_h - \Pi_h\boldsymbol{v}_h\|_K \le C\|(1 - I_h)\boldsymbol{v}_h\|_K \le Ch_K^2|\boldsymbol{v}_h|_{2,K} \le Ch_K\|\nabla\boldsymbol{v}_h\|_K. \tag{4.10}$$

Then a combination of (4.9), (4.10), and approximation theory gives

$$|(\boldsymbol{g}, (1 - \Pi_h)\boldsymbol{v}_h)| = \left|\left(\boldsymbol{g} - P_h^{k-2}\boldsymbol{g}, (1 - \Pi_h)\boldsymbol{v}_h\right)\right| \le Ch^k|\boldsymbol{g}|_{k-1}\|\nabla\boldsymbol{v}_h\|,$$

where $P_h^{k-2}$ is the $L^2$ projection operator onto the space of piecewise polynomials of degree no more than $k-2$. This completes the proof of (2.6).

By Theorem 4.4.4 of [8] we have

$$\|(1-I_h)\boldsymbol{v}_h\|_{\infty,K} + h_K|(1-I_h)\boldsymbol{v}_h|_{1,\infty,K} \le Ch_K|\boldsymbol{v}_h|_{1,\infty,K}, \tag{4.11}$$

for all $K \in \mathcal{T}_h, \boldsymbol{v}_h \in \boldsymbol{V}_h^0$. The inequality (2.7) follows immediately from a combination of the triangle inequality and (4.11).

For (2.8), similarly to (4.10), using (4.11) we have

$$\left\|\Pi_h^{\mathrm{R}}\boldsymbol{v}_h\right\|_{\infty,K} \le C\|(1-I_h)\boldsymbol{v}_h\|_{\infty,K} \le Ch_K|\boldsymbol{v}_h|_{1,\infty,K}.$$

Thus we complete the proof. □

Up to now, we have proven that a class of divergence-free reconstruction operators satisfies the assumptions in Section 2.1. Thus it admits an *a priori* error estimate in Theorem 3. The only question is whether the right-hand side of (3.9) is an $O(h^k)$ quantity if $\boldsymbol{u}$ is sufficiently smooth. The non-trivial terms are the ones corresponding to $\boldsymbol{\eta}_\pi$, $\boldsymbol{\eta}_\pi^1$, $\boldsymbol{\eta}_\pi^{\mathrm{R}}$, and $\|\Delta\boldsymbol{u}\circ(1-\Pi_h)\|_{(\boldsymbol{V}_h^0)'}$. The following lemmas are to answer this question.

**Lemma 6.** *Let $\boldsymbol{u}$ be the solution of (2.9). Suppose that $\boldsymbol{u}(t) \in \boldsymbol{H}^{k+1}(\Omega)$ $(t \in J)$. Then we have*

$$\|\Delta\boldsymbol{u}(t)\circ(1-\Pi_h)\|_{(\boldsymbol{V}_h^0)'} \le Ch^k|\boldsymbol{u}(t)|_{k+1}. \tag{4.12}$$

*Proof.* The inequality (4.12) follows immediately from (2.6) by taking $\boldsymbol{g} = \Delta\boldsymbol{u}(t)$. □

Introduce the seminorm $|||\cdot|||_2$ on $\boldsymbol{H}^2(\mathcal{T}_h)$ by

$$|||\boldsymbol{v}|||_2^2 := \sum_{K\in\mathcal{T}_h} |\boldsymbol{v}|_{2,K}^2 \quad \forall \boldsymbol{v} \in \boldsymbol{H}^2(\mathcal{T}_h).$$

**Lemma 7.** *Let $\boldsymbol{u}$ be the solution of (2.9) and $\boldsymbol{\eta} = \boldsymbol{u} - \Pi_h^{\mathrm{S}}\boldsymbol{u}$. Suppose that $\boldsymbol{u} \in \boldsymbol{H}^{\frac{3}{2}+\epsilon}(\Omega) \cap \boldsymbol{H}^2(\mathcal{T}_h)$ with $\epsilon > 0$. Then we have*

$$\|\boldsymbol{\eta}_\pi\| \le \|\boldsymbol{\eta}\| + C\big(\|\boldsymbol{u} - I_h\boldsymbol{u}\| + \|\boldsymbol{\eta}\| + h^2|||\boldsymbol{\eta}|||_2\big), \tag{4.13}$$

$$\left\|\nabla\boldsymbol{\eta}_\pi^1\right\| \le 2\|\nabla\boldsymbol{\eta}\| + \|\nabla(\boldsymbol{u} - I_h\boldsymbol{u})\| + Ch|||\boldsymbol{\eta}|||_2, \tag{4.14}$$

$$\left\|\boldsymbol{\eta}_\pi^{\mathrm{R}}\right\| \le C\big(\|\boldsymbol{u} - I_h\boldsymbol{u}\| + \|\boldsymbol{\eta}\| + h^2|||\boldsymbol{\eta}|||_2\big), \tag{4.15}$$

*and*

$$|||\boldsymbol{\eta}_\pi^{\mathrm{R}}|||_* \le C(\|\nabla(\boldsymbol{u} - I_h\boldsymbol{u})\| + \|\nabla\boldsymbol{\eta}\| + h|||\boldsymbol{\eta}|||_2). \tag{4.16}$$

*Proof.* Note that

$$\boldsymbol{\eta}_\pi = \boldsymbol{u} - \Pi_h\Pi_h^{\mathrm{S}}\boldsymbol{u} = \boldsymbol{u} - I_h\Pi_h^{\mathrm{S}}\boldsymbol{u} - \Pi_h^{\mathrm{RT}}(1-I_h)\Pi_h^{\mathrm{S}}\boldsymbol{u} = \boldsymbol{\eta} + \big[(1-I_h)\Pi_h^{\mathrm{S}}\boldsymbol{u} - \Pi_h^{\mathrm{RT}}(1-I_h)\Pi_h^{\mathrm{S}}\boldsymbol{u}\big], \tag{4.17}$$

$$\boldsymbol{\eta}_\pi^1 = \boldsymbol{u} - I_h\Pi_h^{\mathrm{S}}\boldsymbol{u} = \boldsymbol{\eta} + (1-I_h)\Pi_h^{\mathrm{S}}\boldsymbol{u}, \tag{4.18}$$

and

$$\boldsymbol{\eta}_\pi^{\mathrm{R}} = -\Pi_h^{\mathrm{R}}\Pi_h^{\mathrm{S}}\boldsymbol{u} = -\Pi_h^{\mathrm{RT}}(1-I_h)\Pi_h^{\mathrm{S}}\boldsymbol{u}. \tag{4.19}$$

A common term in the right-hand sides of (4.17)–(4.19) is

$$(1-I_h)\Pi_h^{\mathrm{S}}\boldsymbol{u} = (\boldsymbol{u} - I_h\boldsymbol{u}) + I_h\boldsymbol{\eta}. \tag{4.20}$$

Note that (4.3) guarantees, together with the triangle inequality,

$$\|I_h \boldsymbol{v}\|_K \leq \|\boldsymbol{v}\|_K + Ch_K^2 |\boldsymbol{v}|_{2,K}, \tag{4.21}$$

and

$$\|\nabla I_h \boldsymbol{v}\|_K \leq \|\nabla \boldsymbol{v}\|_K + Ch_K |\boldsymbol{v}|_{2,K}, \tag{4.22}$$

for all $\boldsymbol{v} \in \boldsymbol{C}^0(\bar{\Omega}) \cap \boldsymbol{H}^2(\mathcal{T}_h), K \in \mathcal{T}_h$. Substituting (4.21) and (4.22) into (4.20) gives

$$\left|(1 - I_h)\Pi_h^{\mathrm{S}} \boldsymbol{u}\right|_{m,K} \leq |\boldsymbol{u} - I_h \boldsymbol{u}|_{m,K} + |\boldsymbol{\eta}|_{m,K} + Ch_K^{2-m} |\boldsymbol{\eta}|_{2,K} \text{ for } m = 0, 1. \tag{4.23}$$

Substituting (4.23) into (4.17)–(4.19) and applying (4.6) for (4.17) and (4.19) provide (4.13)–(4.15).

To estimate $|||\boldsymbol{\eta}_\pi^{\mathrm{R}}|||_*$, with (4.19), (4.6), (4.4), and the inverse inequality one obtains

$$\left\|\boldsymbol{\eta}_\pi^{\mathrm{R}}\right\|_K \leq C\left\|(1 - I_h)\Pi_h^{\mathrm{S}} \boldsymbol{u}\right\|_K \leq Ch_K^2 \left|(1 - I_h)\Pi_h^{\mathrm{S}} \boldsymbol{u}\right|_{2,K} \leq Ch_K \left\|\nabla(1 - I_h)\Pi_h^{\mathrm{S}} \boldsymbol{u}\right\|_K.$$

The above estimate, together with (3.6), (4.23), implies that

$$|||\boldsymbol{\eta}_\pi^{\mathrm{R}}|||_* \leq C\left\|\nabla(1 - I_h)\Pi_h^{\mathrm{S}} \boldsymbol{u}\right\| \leq C(\|\nabla(\boldsymbol{u} - I_h \boldsymbol{u})\| + \|\nabla \boldsymbol{\eta}\| + h|||\boldsymbol{\eta}|||_2).$$

This completes the proof. □

Finally, based on the results in Theorem 3, Lemmas 6 and 7, as well as the approximation properties of $I_h$ and $\Pi_h^{\mathrm{S}}$ [8, 25], we get the convergence rates of the kinetic and dissipation energy errors of $\boldsymbol{u}_h$ (or $\Pi_h \boldsymbol{u}_h$) for (2.12), with the elements and reconstruction operators in this section.

**Corollary 1.** *Let $(\boldsymbol{u}, p)$ be the solution of (2.9) and $(\boldsymbol{u}_h, p_h)$ be the solution of (2.12), with the elements and reconstruction operators used in Section 4. Suppose $\boldsymbol{u} \in L^\infty\left(J; \boldsymbol{H}^{k+1}(\Omega)\right) \cap L^2\left(J; \boldsymbol{W}^{1,\infty}(\Omega)\right)$ and $\boldsymbol{u}_t \in L^2\left(J; \boldsymbol{H}^{k+1}(\Omega)\right)$. Under Assumption 3 and the assumption that $\boldsymbol{u}_h^0 = \Pi_h^{\mathrm{S}} \boldsymbol{u}^0$, the following estimate holds:*

$$\|\boldsymbol{u} - \boldsymbol{u}_h\|_{L^\infty(J;\boldsymbol{L}^2(\Omega))} + \nu^{\frac{1}{2}} \|\nabla(\boldsymbol{u} - \boldsymbol{u}_h)\|_{L^2(J;\boldsymbol{L}^2(\Omega))} \leq B(\boldsymbol{u}, T) h^k, \tag{4.24}$$

*where*

$$\begin{aligned} B(\boldsymbol{u}, T) = C\Big\{ & h|\boldsymbol{u}|_{L^\infty\left(J;\boldsymbol{H}^{k+1}(\Omega)\right)} + |\boldsymbol{u}|_{L^2\left(J;\boldsymbol{H}^{k+1}(\Omega)\right)} + e^{\frac{1}{2}G(\boldsymbol{u},T)} \Big[ hT^{\frac{1}{2}} |\boldsymbol{u}_t|_{L^2\left(J;\boldsymbol{H}^{k+1}(\Omega)\right)} \\ & + |\boldsymbol{u}|_{L^2\left(J;\boldsymbol{H}^{k+1}(\Omega)\right)} + (1 + h)\|\boldsymbol{u}\|^{\frac{1}{2}}_{L^2(J;\boldsymbol{W}^{1,\infty}(\Omega))} |\boldsymbol{u}|_{L^4\left(J;\boldsymbol{H}^{k+1}(\Omega)\right)} \Big] \Big\}, \end{aligned}$$

*with $C$ independent of $p$, $h$, and inverse powers of $\nu$. Here $G(\boldsymbol{u}, T)$ is the same as in Theorem 3.*

The term $\|\boldsymbol{u}\|_{L^2(J;\boldsymbol{W}^{1,\infty}(\Omega))} |\boldsymbol{u}|_{L^4\left(J;\boldsymbol{H}^{k+1}(\Omega)\right)}$ in $B(\boldsymbol{u}, T)$ follows from some Schwarz's inequalities like

$$\int_0^T \|\boldsymbol{u}\|_{1,\infty} \|\boldsymbol{\eta}_\pi\|^2 \, \mathrm{d}t \leq \left( \int_0^T \|\boldsymbol{u}\|_{1,\infty}^2 \, \mathrm{d}t \right)^{\frac{1}{2}} \left( \int_0^T \|\boldsymbol{\eta}_\pi\|^4 \, \mathrm{d}t \right)^{\frac{1}{2}} = \|\boldsymbol{u}\|_{L^2(J;\boldsymbol{W}^{1,\infty}(\Omega))} \|\boldsymbol{\eta}_\pi\|^2_{L^4(J;\boldsymbol{L}^2(\Omega))}.$$

## 5. Numerical experiments

The meaning of some abbreviations used in the legends below is listed in Table 3.

TABLE 3. Some abbreviations used in legends for numerical experiments and their meaning.

| Abbreviations | Meaning |
|---|---|
| BR | Bernardi–Raugel elements [6] |
| TH | Low order Taylor–Hood elements ([32], Sect. 3.6.2) |
| SV2 | Divergence-free second order Scott–Vogelius elements [5] |
| CONV_L-M 2016 | Pressure-robust reconstruction methods in [43] with convective form |
| ROT_L-M 2016 | Pressure-robust reconstruction methods in [43] with rotation form |
| GD | Grad-div stabilization [50] |

### 5.1. Example 1: the lattice vortex problem

In the first example, we consider the lattice vortex problem [49, 55] on $\Omega = (0,1)^2$. The exact velocity is set as

$$\boldsymbol{u}(t,\boldsymbol{x}) = \boldsymbol{u}^0(\boldsymbol{x})\exp\bigl(-8\pi^2\nu t\bigr),$$

with

$$\boldsymbol{u}^0(\boldsymbol{x}) = \bigl(\sin(2\pi x)\sin(2\pi y), \cos(2\pi x)\cos(2\pi y)\bigr)^{\mathrm{T}}$$

with an appropriate $p$, $\boldsymbol{u}$ fulfills an exact unsteady NSE with $\boldsymbol{f} = \boldsymbol{0}$. We choose a small $\nu$ and a large $T$: $\nu = 1\times 10^{-5}$ and $T = 10$.

We do some numerical experiments by Bernardi–Raugel elements on an unstructured mesh with 14 112 triangles and 49 778 DoFs. To make a comparison, the EMAC formulation and the pressure-robust reconstruction method in [43] with the rotation formulation are also tested. Further, considering that the low order Taylor–Hood element is much more popular in practice, we also show some results from this element with EMAC and/or the grad-div stabilization. The well-known second order Scott–Vogelius (SV2) element, $\boldsymbol{P}_2/P_1^{\mathrm{disc}}$ [5, 34], with the convective formulation, is also used to make a comparison, which is a kind of divergence-free method. We try to make all the methods have almost the same number of DoFs. The methods with Taylor–Hood element and SV2 element are run on a mesh with 11 018 triangles (50 154 DoFs) and a barycentric-refined mesh with 7068 triangles (49 686 DoFs), respectively. For the time discretizations, we use the BDF2 scheme with $\Delta t = 0.001$. At each time step we solve a nonlinear system by the Newton iteration method with a tolerance of $10^{-8}$ in the $H^1$ norm.

We also do some comparison between the results from different $\alpha$. And for $\alpha = 1$ we try two cases: the full $\alpha$-related stabilization and the only left-hand one. The latter means that the $\alpha$-related stabilization is only added to the coefficient matrix, that is, $\alpha\Delta t^{-1}(\frac{3}{2}\Pi_h^{\mathrm{R}}\boldsymbol{u}_h^n, \Pi_h^{\mathrm{R}}\boldsymbol{v}_h)$ is employed but $\alpha\Delta t^{-1}(2\Pi_h^{\mathrm{R}}\boldsymbol{u}_h^{n-1} - \frac{1}{2}\Pi_h^{\mathrm{R}}\boldsymbol{u}_h^{n-2}, \Pi_h^{\mathrm{R}}\boldsymbol{v}_h)$ is not for the time step $t^n$. In the legends we use "$\alpha = 1$ (L)" to represent this case. For other $\alpha$ we only use the full one.

Some results are shown in Figures 1–3. From Figure 1 one can see the errors of EMAC and pressure-robust ROT formulations with the Bernardi–Raugel element grow quickly at an early time. We conjecture that the reason for EMAC is that it is not pressure-robust and the reason for pressure-robust ROT is that it is not Re-semi-robust. The former can be considerably improved by using the low order Taylor–Hood element, since its pressure approximation order is one order higher than Bernardi–Raugel pressure (but the number of DoFs of the pressure is instead less due to the continuity). For all the methods in Figure 1, EMAPR with $\alpha = 1$ (only left-hand) shows best performance. And the cost of this method is also the second least (see Tab. 4).

In Figure 2 we show some comparison with the grad-div stabilized EMAC (the stabilization coefficient is always taken to be 0.1) and Taylor–Hood elements. We also consider a more complicated pressure there, by setting $\boldsymbol{f} = 10^2\nabla(xy), 10^3\nabla(xy)$. Note that this changes the pressure but not the velocity. Without a modified continuous pressure, the grad-div stabilized EMAC gives a better performance than our method. However, as the pressure becomes more complicated, its performance becomes worse. For EMAPR method, more complicated pressures do not affect the discrete velocity.

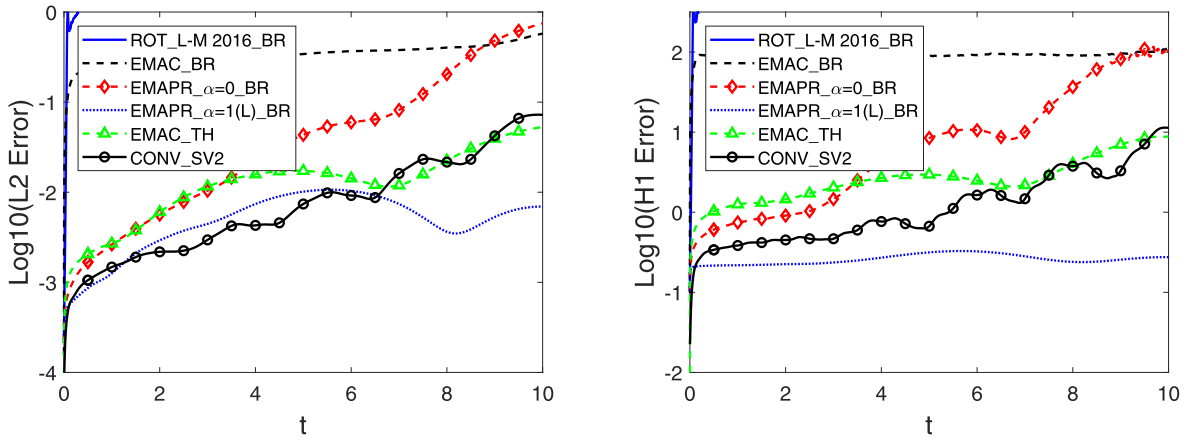


FIGURE 1. Example 1. $L^2$ errors (*left*) and $H^1$ errors (*right*) over time for different variants/modifications of the Bernardi–Raugel finite element method, Taylor–Hood finite element method with EMAC form, and Scott–Vogelius finite element method with convective form.

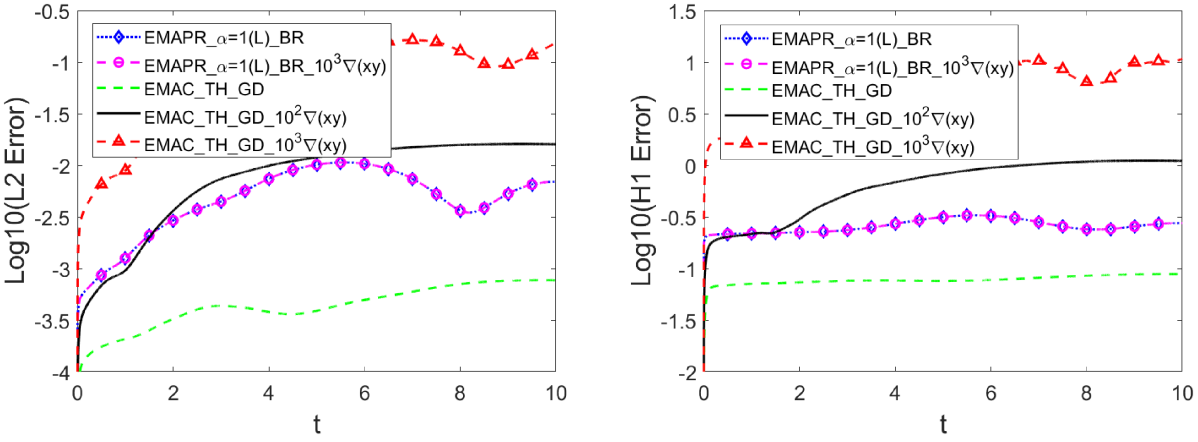


FIGURE 2. Example 1. $L^2$ errors (*left*) and $H^1$ errors (*right*) over time for the Bernardi–Raugel finite element method with EMAPR reconstruction ($\boldsymbol{f} = 0, 10^3\nabla(xy)$) and Taylor–Hood finite element method with EMAC form and grad-div stabilization ($\boldsymbol{f} = 0, 10^2\nabla(xy), 10^3\nabla(xy)$).

From Figure 3 one can see the results from $\alpha = 0$ and $\alpha = 10^{-3}$ are virtually the same, which further verify that a small $\alpha$ is not a meaningful choice. The full stabilization with $\alpha = 10^3$ gives the best accuracy before $t = 8$, while the only left-hand stabilization with $\alpha = 1$ performs best at the final time.

## 5.2. Example 2: potential flow

For the second example we consider the potential flow in Example 6 of [43]. On $\Omega = (0,1)^2$ the velocity is prescribed as $\boldsymbol{u} = \min\{t, 1\}\nabla\chi$ with $\chi = x^3y - y^3x$. We set $\boldsymbol{f} = 0$ such that the pressure gradient exactly balances the gradient filed produced by the velocity terms. Due to the quadratic convective term, the pressure is much more complicated than the velocity [24]. The pressure-robustness will play a key role on the accuracy of the simulations of this problem.

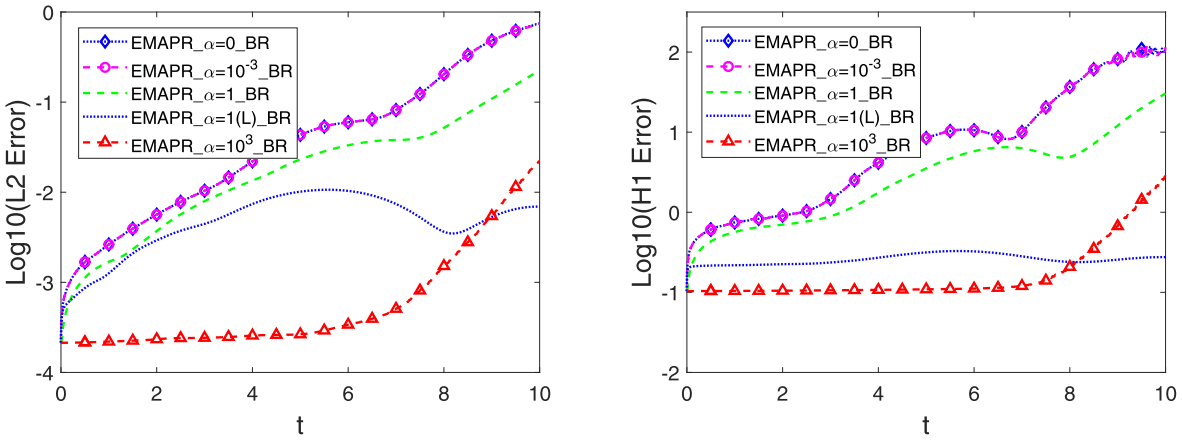


FIGURE 3. Example 1. $L^2$ errors (*left*) and $H^1$ errors (*right*) over time for the Bernardi–Raugel finite element method with EMAPR reconstruction and different parameters/choices of the stabilization.

TABLE 4. The CPU time cost of some methods in Example 1. The "Total iterations" term refers to the total number of Newton iteration steps.

| Methods | Total cost (s) | Total iterations | Cost per iteration (s) |
|---|---|---|---|
| EMAC_BR | 36 971 | 30 048 | 1.2304 |
| EMAPR_$\alpha = 0$_BR | 27 466 | 21 792 | 1.2604 |
| EMAPR_$\alpha = 1$(L)_BR | 23 904 | 20 000 | 1.1952 |
| EMAC_TH | 34 749 | 20 001 | 1.7374 |
| CONV_SV2 | 17 923 | 20 000 | 0.8961 |

TABLE 5. Example 2. Errors for different variants/modifications of the Bernardi–Raugel finite element method (classical CONV/EMAPR_$\alpha = 0$/CONV_L-M 2016).

| $t$ | $\|\boldsymbol{u} - \boldsymbol{u}_h\|$ | $\|\nabla(\boldsymbol{u} - \boldsymbol{u}_h)\|$ | $\|P_h p - p_h\|$ |
|---|---|---|---|
| 0.5 | 1.84e−2/1.61e−4/1.62e−4 | 3.66/3.72e−2/3.86e−2 | 1.63e−2/5.02e−5/4.70e−5 |
| 1 | 4.35e−2/4.47e−4/4.71e−4 | 8.47/8.73e−2/9.83e−2 | 5.59e−2/2.46e−4/2.29e−4 |
| 1.5 | 5.50e−2/5.56e−4/6.07e−4 | 9.24/8.89e−2/0.10 | 4.02e−2/2.62e−4/2.37e−4 |
| 2.0 | 5.53e−2/5.98e−4/7.37e−4 | 9.24/8.90e−2/0.10 | 4.09e−2/2.84e−4/2.68e−4 |

We consider the case of $\nu = 5 \times 10^{-4}$ and apply the Bernardi–Raugel element and the second order element in Table 1, $\boldsymbol{P}_2^{\text{bubble}}/P_1^{\text{disc}}$. For the time-stepping, the BDF2 scheme is used. A non-uniform mesh is used, which consists of 2112 triangles and produces total 7562 DoFs for Bernardi–Raugel element and 19 234 DoFs for $\boldsymbol{P}_2^{\text{bubble}}/P_1^{\text{disc}}$. We set $\Delta t = 0.01$ and $T = 2$. We also give some results from the classical scheme and the pressure-robust reconstruction scheme in [43] with the convective form for the nonlinear term. In each time step, we solve a linear problem by replacing the advective velocity in trilinear forms with a linear extrapolation of the previous step velocities ($\boldsymbol{u}_h^n \approx 2\boldsymbol{u}_h^{n-1} - \boldsymbol{u}_h^{n-2}$). Some results are shown in Tables 5 and 6. All the pressure-robust schemes have a much better accuracy than the classical scheme.

TABLE 6. Example 2. Errors for different variants/modifications of $\boldsymbol{P}_2^{\text{bubble}}/P_1^{\text{disc}}$ finite element method (classical CONV/EMAPR_$\alpha = 0$/CONV_L-M 2016).

| $t$ | $\|\boldsymbol{u} - \boldsymbol{u}_h\|$ | $\|\nabla(\boldsymbol{u} - \boldsymbol{u}_h)\|$ | $\|P_h p - p_h\|$ |
|---|---|---|---|
| 0.5 | 4.85e−5/1.61e−6/1.20e−6 | 1.21e−2/4.55e−4/3.36e−4 | 6.94e−5/1.09e−6/5.80e−7 |
| 1 | 9.81e−5/4.95e−6/3.40e−6 | 2.58e−2/1.34e−3/8.69e−4 | 1.50e−4/5.14e−6/2.54e−6 |
| 1.5 | 1.15e−4/5.75e−6/3.80e−6 | 2.65e−2/1.36e−3/8.95e−4 | 1.44e−4/5.29e−6/2.64e−6 |
| 2.0 | 1.17e−4/6.07e−6/3.94e−6 | 2.66e−2/1.37e−3/8.98e−4 | 1.43e−4/5.47e−6/2.73e−6 |

### 5.3. Example 3: flow passing a cylinder in two dimensions

This example describes a time-dependent flow passing a cylinder in two dimensions [31,54]. The computational domain is set as

$$\Omega = (0, 2.2) \times (0, 0.41) \setminus \left\{(x, y) \mid (x - 0.2)^2 + (y - 0.2)^2 \le 0.05^2\right\}$$

and the final time is $T = 8$. The parabolic inflow and outflow boundary conditions are given by

$$\boldsymbol{u}(0, y) = \boldsymbol{u}(2.2, y) = 0.41^{-2} \sin(\pi t/8)(6y(0.41 - y), 0)^{\top},$$

such that the mean inflow/outflow speed is $U(t) = \sin(\pi t/8)$ and $\max_{0\le t\le 8} U(t) = 1$. On all other boundaries the no-slip boundary condition ($\boldsymbol{u} = \boldsymbol{0}$) is enforced. The external force is $\boldsymbol{f} = \boldsymbol{0}$ and the viscosity is $\nu = 10^{-3}$ such that the Reynolds number Re satisfies $0 \le \text{Re} \le 100$. The flow starts with static ($\boldsymbol{u}^0 = \boldsymbol{0}$). In this example a vortex street develops behind the cylinder around $t = 4$ [31].

The geometry setting and the mesh we used can be found in Figure 4. We employee the Bernardi–Raugel element to check the performance of our method, whose number of DoFs is 41368. The second order Scott–Vogelius pair (with the standard convective form for the nonlinear discretization) is used as a reference and comparison, which runs on the barycentric refinement of the mesh in Figure 4, producing totally 245 898 DoFs. For time discretizaton, the BDF2 method is used with $\Delta t = 0.0025$. On each time step a linearized system is solved by replacing the advective velocity $\boldsymbol{u}_h^n$ with a linear extrapolation $\mathcal{L}(\boldsymbol{u}_h^{n-1}, \boldsymbol{u}_h^{n-2}) := 2\boldsymbol{u}_h^{n-1} - \boldsymbol{u}_h^{n-2}$. Quantities of interest are drag and lift forces. Following the strategy in [31,33,49], the drag and lift are computed *via*

$$c_d(t^n) = -20\left(\frac{1}{2\Delta t} t_h(\boldsymbol{u}_h, \boldsymbol{v}_d) + \nu(\nabla \boldsymbol{u}_h^n, \nabla \boldsymbol{v}_d) + c^\star\big(\mathcal{L}(\boldsymbol{u}_h^{n-1}, \boldsymbol{u}_h^{n-2}), \boldsymbol{u}_h^n, \boldsymbol{v}_d\big) - (p^n, \nabla \cdot \boldsymbol{v}_d)\right),$$
$$c_l(t^n) = -20\left(\frac{1}{2\Delta t} t_h(\boldsymbol{u}_h, \boldsymbol{v}_l) + \nu(\nabla \boldsymbol{u}_h^n, \nabla \boldsymbol{v}_l) + c^\star\big(\mathcal{L}(\boldsymbol{u}_h^{n-1}, \boldsymbol{u}_h^{n-2}), \boldsymbol{u}_h^n, \boldsymbol{v}_l\big) - (p^n, \nabla \cdot \boldsymbol{v}_l)\right),$$

where $t_h(\boldsymbol{u}_h, \boldsymbol{v}_h) = d_h(3\boldsymbol{u}_h^n - 4\boldsymbol{u}_h^{n-1} + \boldsymbol{u}_h^{n-2}, \boldsymbol{v}_h)$ and $c^\star = c_h$ for the Bernardi–Raugel element and $t_h(\boldsymbol{u}_h, \boldsymbol{v}_h) = (3\boldsymbol{u}_h^n - 4\boldsymbol{u}_h^{n-1} + \boldsymbol{u}_h^{n-2}, \boldsymbol{v}_h)$ and $c^\star = c$ for the Scott–Vogelius element.

Some contours of speed can be found in Figure 5. The results from our method is very close to those from the Scott–Vogelius element method, and they are all very close to the plots in Figure 6 from [18]. Some values corresponding to maximum drag and lift are listed in Table 7. We try different $\alpha$ from 0 to $10^3$. In the paper [54], the reference intervals of maximum drag and lift are given as $[2.93, 2.97]$ and $[0.47, 0.49]$, respectively. It seems that the $\alpha$-related stabilization is not necessary for this example. One possible reason is that this is a low Reynolds number flow. Our methods with $\alpha = 0, 0.1, 1$ give very similar results. On the other hand, we also find that for a larger $\alpha$ ($\alpha = 10, 10^3$) the maximal lift coefficient can fall outside of the reference interval $[0.47, 0.49]$, which implies that the choice of $\alpha$ does have an influence on the performance of our method, although this influence seems to be not large here. We conjecture that for low Reynolds number flows a small $\alpha$ ($\alpha \le 1$) is sufficient and a larger $\alpha$ is not recommended.

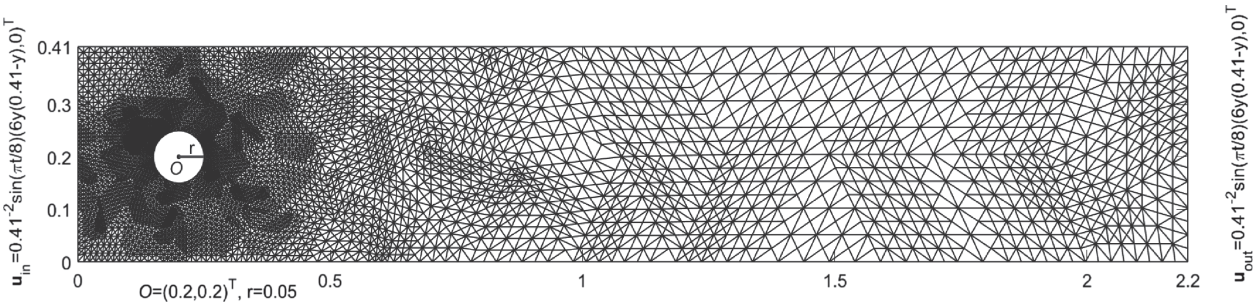


FIGURE 4. Example 3. Geometry setting, inflow/outflow conditions, and mesh.

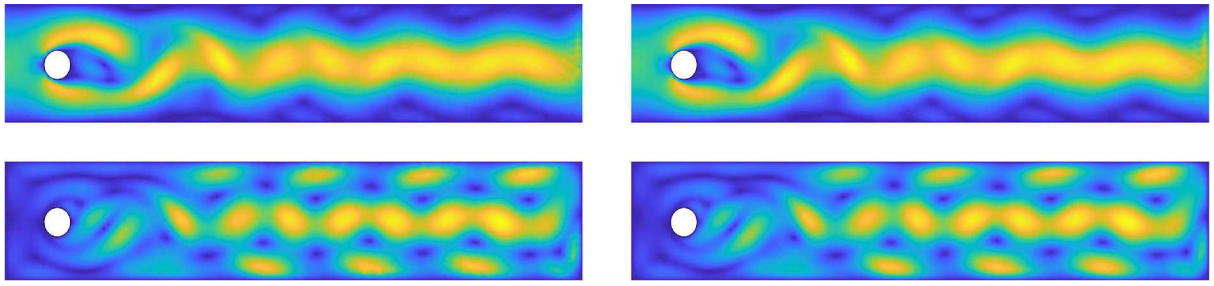

FIGURE 5. Example 3. Speed contours for $t = 7, 8$ (from *top* to *bottom*) for the Bernardi–Raugel finite element method with EMAPR reconstruction ($\alpha = 0$, *left*) and Scott–Vogelius finite element method with convective form (*right*).

TABLE 7. Example 3. Maximal values of drag and lift for the Bernardi–Raugel finite element method with EMAPR reconstruction and different choices of $\alpha$ and Scott–Vogelius finite element method with convective form.

| Method | Total DoFs | $\Delta t$ | $t(c_{d,\max})$ | $c_{d,\max}$ | $t(c_{l,\max})$ | $c_{l,\max}$ |
|---|---|---|---|---|---|---|
| EMAPR_$\alpha = 0$_BR | 41 368 | 0.0025 | 3.9375 | 2.9534 | 5.6925 | 0.4870 |
| EMAPR_$\alpha = 0.1$_BR | 41 368 | 0.0025 | 3.9375 | 2.9534 | 5.6925 | 0.4871 |
| EMAPR_$\alpha = 1$_BR | 41 368 | 0.0025 | 3.9375 | 2.9534 | 5.6925 | 0.4884 |
| EMAPR_$\alpha = 10$_BR | 41 368 | 0.0025 | 3.9375 | 2.9533 | 5.6925 | 0.4940 |
| EMAPR_$\alpha = 10^3$_BR | 41 368 | 0.0025 | 3.9525 | 2.9308 | 5.6900 | 0.4981 |
| CONV_SV2 | 245 898 | 0.0025 | 3.9350 | 2.9397 | 5.6900 | 0.4754 |

## 6. CONCLUSIONS

We have developed an EMA-conserving, pressure-robust and Re-semi-robust reconstruction method for a class of finite element methods of the Navier–Stokes equations. The lowest order case is the Bernardi–Raugel element. In practice, we conjecture grad-div stabilized EMAC is a very simple and efficient method in many situations. However, when the pressure is much larger or more complicated than the velocity, besides divergence-

free elements, we believe that the method proposed herein can also be a good choice due to its easier construction and mild requirement of the meshes. Further research on stabilizations is an important part of future work.

*Acknowledgements.* This work was supported by the National Natural Science Foundation of China (Grant 12131014). The first author was also supported by the China Scholarship Council (Grant 202106220106).

## References

[1] R. Abramov and A. Majda, Discrete approximations with additional conserved quantities: deterministic and statistical behavior. *Methods Appl. Anal.* **10** (2003) 151–190.

[2] N. Ahmed, A. Linke and C. Merdon, On really locking-free mixed finite element methods for the transient incompressible stokes equations. *SIAM J. Numer. Anal.* **56** (2018) 185–209.

[3] A. Allendes, G.R. Barrenechea and J. Novo, A divergence-free stabilized finite element method for the evolutionary Navier–Stokes equations. *SIAM J. Sci. Comput.* **43** (2021) A3809–A3836.

[4] A. Arakawa, Computational design for long-term numerical integration of the equations of fluid motion: two dimensional incompressible flow, Part I. *J. Comput. Phys.* **1** (1966) 119–143.

[5] D.N. Arnold and J. Qin, Quadratic velocity/linear pressure Stokes elements, in Advances in Computer Methods for Partial Differential Equations-VII, edited by R. Vichnevetsky, D. Knight and G. Richter. IMACS, New Brunswick, NJ (1992) 28–34.

[6] C. Bernardi and G. Raugel, Analysis of some finite elements for the Stokes problem. *Math. Comp.* **44** (1985) 71–79.

[7] D. Boffi, F. Brezzi and M. Fortin, Mixed Finite Element Methods and Applications. Vol. 44 of *Springer Series in Computational Mathematics*. Springer Berlin Heidelberg, Heidelberg (2013).

[8] S.C. Brenner and L.R. Scott, The Mathematical Theory of Finite Element Methods. Vol. 15 of *Texts in Applied Mathematics*. Springer New York, New York, NY (2008).

[9] F. Brezzi, T.J.R. Hughes, L.D. Marini and A. Masud, Mixed discontinuous Galerkin methods for Darcy flow. *J. Sci. Comput.* **22–23** (2005) 119–145.

[10] E. Burman and M.A. Fernández, Continuous interior penalty finite element method for the time-dependent Navier–Stokes equations: space discretization and convergence. *Numer. Math.* **107** (2007) 39–77.

[11] M.A. Case, V.J. Ervin, A. Linke and L.G. Rebholz, A connection between Scott–Vogelius and grad-div stabilized Taylor–Hood FE approximations of the Navier–Stokes equations. *SIAM J. Numer. Anal.* **49** (2011) 1461–1481.

[12] S. Charnyi, T. Heister, M.A. Olshanskii and L.G. Rebholz, On conservation laws of Navier–Stokes Galerkin discretizations. *J. Comput. Phys.* **337** (2017) 289–308.

[13] S. Charnyi, T. Heister, M.A. Olshanskii and L.G. Rebholz, Efficient discretizations for the EMAC formulation of the incompressible Navier–Stokes equations. *Appl. Numer. Math.* **141** (2019) 220–233.

[14] S.H. Christiansen and K. Hu, Generalized finite element systems for smooth differential forms and Stokes' problem. *Numer. Math.* **140** (2018) 327–371.

[15] B. Cockburn, G. Kanschat and D. Schötzau, A note on discontinuous Galerkin divergence-free solutions of the Navier–Stokes equations. *J. Sci. Comput.* **31** (2007) 61–73.

[16] J. de Frutos, B. García-Archilla, V. John and J. Novo, Analysis of the grad-div stabilization for the time-dependent Navier–Stokes equations with inf-sup stable finite elements. *Adv. Comput. Math.* **44** (2018) 195–225.

[17] J. de Frutos, B. García-Archilla, V. John and J. Novo, Error analysis of non inf-sup stable discretizations of the time-dependent Navier–Stokes equations with local projection stabilization. *IMA J. Numer. Anal.* **39** (2019) 1747–1786.

[18] J. de Frutos, B. García-Archilla and J. Novo, Fully discrete approximations to the time-dependent Navier–Stokes equations with a projection method in time and grad-div stabilization. *J. Sci. Comput.* **80** (2019) 1330–1368.

[19] J.A. Evans and T.J.R. Hughes, Isogeometric divergence-conforming B-splines for the unsteady Navier–Stokes equations. *J. Comput. Phys.* **241** (2013) 141–167.

[20] G.J. Fix, Finite element models for ocean circulation problems. *SIAM J. Appl. Math.* **29** (1975) 371–387.

[21] K.J. Galvin, A. Linke, L.G. Rebholz and N.E. Wilson, Stabilizing poor mass conservation in incompressible flow problems with large irrotational forcing and application to thermal convection. *Comput. Methods Appl. Mech. Eng.* **237–240** (2012) 166–176.

[22] B. García-Archilla, V. John and J. Novo, On the convergence order of the finite element error in the kinetic energy for high Reynolds number incompressible flows. *Comput. Methods Appl. Mech. Eng.* **385** (2021) 114032.

[23] B. García-Archilla, V. John and J. Novo, Symmetric pressure stabilization for equal-order finite element approximations to the time-dependent Navier–Stokes equations. *IMA J. Numer. Anal.* **41** (2021) 1093–1129.

[24] N.R. Gauger, A. Linke and P.W. Schroeder, On high-order pressure-robust space discretisations, their advantages for incompressible high Reynolds number generalised Beltrami flows and beyond. *SMAI J. Comput. Math.* **5** (2019) 89–129.

[25] V. Girault and P.-A. Raviart, Finite Element Methods for Navier–Stokes Equations. Vol. 5 of *Springer Series in Computational Mathematics*. Springer Berlin Heidelberg, Berlin, Heidelberg (1986).

[26] V. Girault, R.H. Nochetto and L.R. Scott, Max-norm estimates for Stokes and Navier–Stokes approximations in convex polyhedra. *Numer. Math.* **131** (2015) 771–822.

[27] J. Guzmán and M. Neilan, A family of nonconforming elements for the Brinkman problem. *IMA J. Numer. Anal.* **32** (2012) 1484–1508.

[28] J. Guzmán and M. Neilan, Conforming and divergence-free Stokes elements on general triangular meshes. *Math. Comp.* **83** (2013) 15–36.

[29] J. Guzmán and M. Neilan, Conforming and divergence-free Stokes elements in three dimensions. *IMA J. Numer. Anal.* **34** (2014) 1489–1508.

[30] J. Guzmán and M. Neilan, Inf-sup stable finite elements on barycentric refinements producing divergence–free approximations in arbitrary dimensions. *SIAM J. Numer. Anal.* **56** (2018) 2826–2844.

[31] V. John, Reference values for drag and lift of a two-dimensional time-dependent flow around a cylinder. *Int. J. Numer. Meth. Fluids* **44** (2004) 777–788.

[32] V. John, Finite Element Methods for Incompressible Flow Problems. Springer, Cham (2016).

[33] V. John and S. Kaya, A finite element variational multiscale method for the Navier–Stokes equations. *SIAM J. Sci. Comput.* **26** (2005) 1485–1503.

[34] V. John, A. Linke, C. Merdon, M. Neilan and L.G. Rebholz, On the divergence constraint in mixed finite element methods for incompressible flows. *SIAM Rev.* **59** (2017) 492–544.

[35] V. John, P. Knobloch and J. Novo, Finite elements for scalar convection-dominated equations and incompressible flow problems: a never ending story? *Comput. Visual Sci.* **19** (2018) 47–63.

[36] J. Könnö and R. Stenberg, $H(\mathrm{div})$-conforming finite elements for the Binkman problem. *Math. Models Methods Appl. Sci.* **21** (2011) 2227–2248.

[37] P.L. Lederer, *Pressure-robust discretizations for Navier–Stokes equations: divergence-free reconstruction for Taylor–Hood elements and high order hybrid discontinuous Galerkin methods*. Master's thesis, Vienna Technical University, Vienna (2016).

[38] P.L. Lederer, A. Linke, C. Merdon and J. Schöberl, Divergence-free reconstruction operators for pressure-robust Stokes discretizations with continuous pressure finite elements. *SIAM J. Numer. Anal.* **55** (2017) 1291–1314.

[39] P.L. Lederer, C. Lehrenfeld and J. Schöberl, Hybrid discontinuous Galerkin methods with relaxed $H(\mathrm{div})$-conformity for incompressible flows. Part II. *ESAIM: Math. Model. Numer. Anal.* **53** (2019) 503–522.

[40] P.L. Lederer, C. Merdon and J. Schöberl, Refined a posteriori error estimation for classical and pressure-robust Stokes finite element methods. *Numer. Math.* **142** (2019) 713–748.

[41] A. Linke, On the role of the Helmholtz decomposition in mixed methods for incompressible flows and a new variational crime. *Comput. Methods Appl. Mech. Eng.* **268** (2014) 782–800.

[42] A. Linke and C. Merdon, On velocity errors due to irrotational forces in the Navier–Stokes momentum balance. *J. Comput. Phys.* **313** (2016) 654–661.

[43] A. Linke and C. Merdon, Pressure-robustness and discrete Helmholtz projectors in mixed finite element methods for the incompressible Navier–Stokes equations. *Comput. Methods Appl. Mech. Eng.* **311** (2016) 304–326.

[44] A. Linke and L.G. Rebholz, Pressure-induced locking in mixed methods for time-dependent Navier–Stokes equations. *J. Comput. Phys.* **388** (2019) 350–356.

[45] A. Linke, G. Matthies and L. Tobiska, Robust arbitrary order mixed finite element methods for the incompressible Stokes equations with pressure independent velocity errors. *ESAIM: Math. Model. Numer. Anal.* **50** (2016) 289–309.

[46] M. Neilan, Discrete and conforming smooth de Rham complexes in three dimensions. *Math. Comp.* **84** (2015) 2059–2081.

[47] M. Neilan and B. Otus, Divergence-free Scott–Vogelius elements on curved domains. *SIAM J. Numer. Anal.* **59** (2021) 1090–1116.

[48] M.A. Olshanskii, A low order Galerkin finite element method for the Navier–Stokes equations of steady incompressible flow: a stabilization issue and iterative methods. *Comput. Methods Appl. Mech. Eng.* **191** (2002) 5515–5536.

[49] M.A. Olshanskii and L.G. Rebholz, Longer time accuracy for incompressible Navier–Stokes simulations with the EMAC formulation. *Comput. Methods Appl. Mech. Eng.* **372** (2020) 113369.

[50] M.A. Olshanskii and A. Reusken, Grad-div stabilization for Stokes equations. *Math. Comp.* **73** (2004) 1699–1718.

[51] A. Palha and M. Gerritsma, A mass, energy, enstrophy and vorticity conserving (MEEVC) mimetic spectral element discretization for the 2D incompressible Navier–Stokes equations. *J. Comput. Phys.* **328** (2017) 200–220.

[52] L.G. Rebholz, An energy- and helicity-conserving finite element scheme for the Navier–Stokes equations. *SIAM J. Numer. Anal.* **45** (2007) 1622–1638.

[53] S. Rhebergen and G.N. Wells, An embedded-hybridized discontinuous Galerkin finite element method for the Stokes equations. *Comput. Methods Appl. Mech. Eng.* **358** (2020) 112619.

[54] M. Schäfer, S. Turek, F. Durst, E. Krause and R. Rannacher, Benchmark Computations of Laminar Flow Around a Cylinder. Vieweg+Teubner Verlag, Wiesbaden (1996) 547–566.

[55] P.W. Schroeder, C. Lehrenfeld, A. Linke and G. Lube, Towards computable flows and robust estimates for inf-sup stable FEM applied to the time-dependent incompressible Navier–Stokes equations. *SeMA* **75** (2018) 629–653.

[56] J. Wang and X. Ye, New finite element methods in computational fluid dynamics by $H(\mathrm{div})$ elements. *SIAM J. Numer. Anal.* **45** (2007) 1269–1286.

[57] J. Wang, X. Wang and X. Ye, Finite element methods for the Navier–Stokes equations by $H(\mathrm{div})$ elements. *J. Comput. Math.* **26** (2008) 410–436.

[58] S. Zhang, A new family of stable mixed finite elements for the 3D Stokes equations. *Math. Comp.* **74** (2005) 543–554.